CHAPTER 6

LOPINAVIR

6.1 BACKGROUND

Lopinavir (figure 6.1) is a peptidomimetic drug, which inhibits the HIV protease enzyme from cleaving the Gag-Pol polyprotein, resulting in the production of immature, non-infectious viral particles (Safrin, 2004:818). Sham *et al*. (1998:3218) of Abbott Laboratories investigated lopinavir, back then still known by its laboratory code, ABT-378, as an alternative protease inhibitor for treatment of patients whose HIV protease had become resistant to ritonavir. The research was based on the work of Molla *et al.* (1996:760) who had already identified the mutations responsible for HIV protease resistance to ritonavir. Mutants at valine-82 appeared first in most patients, and although this mutation on its own was not deemed significant to confer resistance, it retained susceptibility to structurally diverse protease inhibitors. This suggested that duel protease inhibitor treatment might increase the duration of viral suppression.

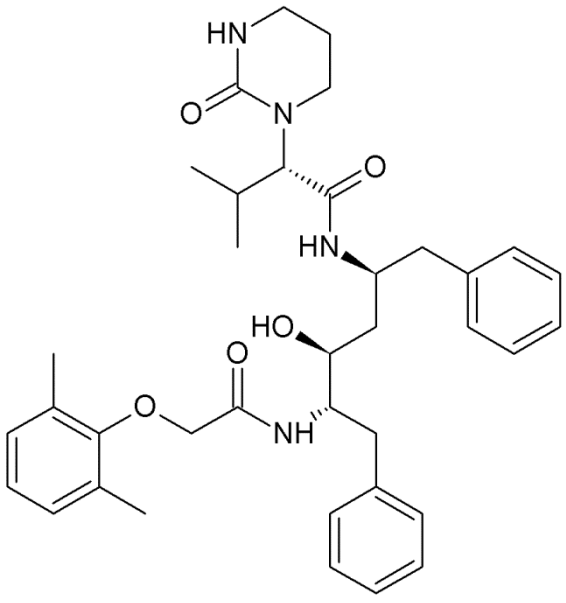

Figure 6.1: Lopinavir, adapted from Sham *et al*. (1998:3221).

Sham *et al*. (1998:3219) set about designing ABT-378 (lopinavir) and two other protease inhibitors (A-155704 and A-155564) based on the single crystal x-ray diffraction (SXRD) data of the complex of HIV-1 protease with ritonavir reported by Kempf *et al*. (1995:2487).

Table 6.1: The activities of HIV protease inhibitors leading to the identification of lopinavir, adapted from Sham *et al.* (1998:3221)

Protease inhibitor	**Structure**	**% protease inhibition at 0.5 nM**	**EC_{50} (µM) in the presence of**	
			0% HS	**50% HS**
Ritonavir	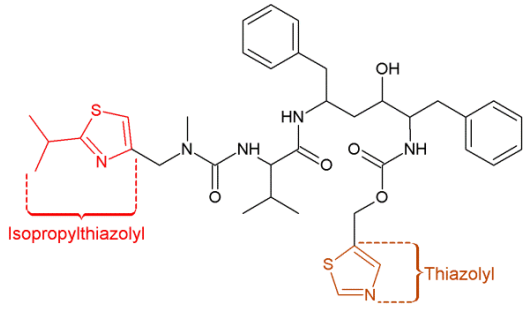	79	0.06	1.04
A-155704	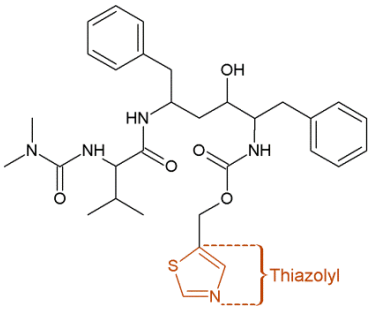	49	1.8	4.2
A-155564	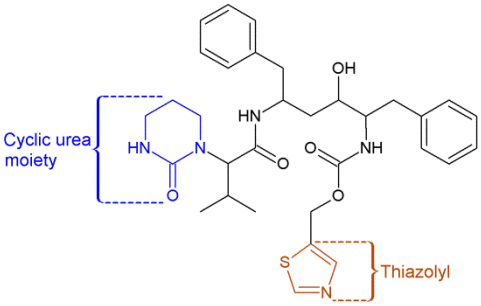	79	0.15	0.64
ABT-378 (Lopinavir)	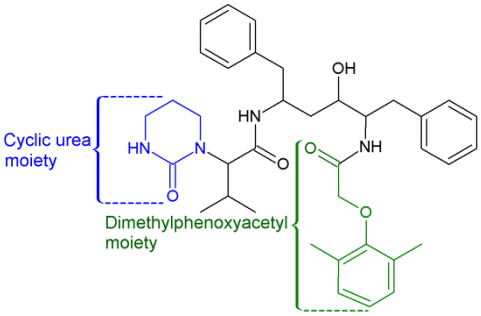	93	0.017	0.10

The SXRD analysis of this complex revealed a hydrophobic interaction between the isopropyl side chain of Val-82 and the isopropyl substituent projecting from the 2 position of the P3 thiazolyl group of ritonavir. Mutations at Val-82 to alanine, threonine or phenylalanine (Molla *et al*., 1996:760), decrease the affinity of ritonavir for the active site. The aim, for Sham *et al*. (1998:3219), was to design new protease inhibitors which were less dependent on an interaction with Val-82, the results of which are given in table 6.1. Apart from assessing the protease inhibition, the *in vitro* HIV assay also contained 50% human serum (HS) to investigate the effect of serum binding on the antiviral potency. To start with, the P3 isopropylthiazolyl group of ritonavir was eliminated, yielding compound A-155704, which displayed a significant loss of affinity for wild-type HIV protease and a 30-fold loss in anti-HIV activity compared to ritonavir. The serum binding of A-155704 was also higher. To increase conformational constraint, a cyclic urea moiety was introduced to compound A-155564, which exhibited an increase in anti-HIV activity while maintaining a low level of serum binding. Finally, replacement of the peripheral thiazolyl group with a dimethylphenoxyacetyl moiety gave ABT-378 (lopinavir), which inhibited 93% of wild-type HIV protease activity at 0.5 nM while displaying the lowest serum binding levels of all the compounds tested. It also had a $>10^5$-fold specificity for HIV protease over mammalian aspartic proteinases renin, cathepsin D and cathepsin E.

Sham *et al*. (1998:3220) also tested lopinavir against mutated HIV protease from patients who were known to have developed resistance against ritonavir. Although the activity of lopinavir declined against these multiply mutated HIV protease strains, the EC_{50} values were still 6-, 13- and 9-fold higher than those against corresponding baseline viruses compared to the 28-, 41- and 17-fold higher values of ritonavir in the same three patients tested. HIV isolates from nine different patients containing three or more mutations were also tested for susceptibility to lopinavir. The EC_{50} of lopinavir against these isolates was 10-fold lower than that of ritonavir, and in most cases, similar or only slightly higher than the EC_{50} of ritonavir against baseline (wild-type) isolates.

Kempf *et al*. (1997:655) studied ritonavir's inhibitory effects on CYP-mediated metabolism of HIV protease inhibitors; saquinavir, indinavir, nelfinavir and the experimental drug VX-478, in order to enhance the pharmacokinetics of these drugs. It is obvious that protease inhibitors would have an undesirable pharmacokinetic profile, because of poor absorption and rapid hepatobiliary elimination due to their peptidomimetic structure. Their studies showed that ritonavir exerted its pharmacokinetic enhancement activity through potent inhibition of CYP3A, and to a lesser extent CYP2D6. Ritonavir inhibited the metabolism of saquinavir in human liver microsomes with an IC_{50} value of 0.25 μM, 8-fold lower than that of the known

CYP3A inhibitor ketoconazole for the same drug. The IC_{50} values for indinavir, nelfinavir and VX-478 were 2.2, 0.62 and 0.1 μM respectively. Based on these findings, Sham *et al.* (1998:3221) decided to investigate the *in vitro* inhibition of lopinavir metabolism by ritonavir. Using rat and human liver microsomal preparations, they found that lopinavir was metabolised almost exclusively by the 3A4 isozyme of CYP. Ritonavir inhibited this metabolism, with IC_{50} values of 0.036 and 0.073 μM in rat and human liver microsomes respectively. In human studies, administration of lopinavir alone as a single drug gave only a brief plasma concentration exceeding 0.1 μg/ml which declined to <0.01 μg/ml over 8 hours. However, coadministration of lopinavir with a small amount of ritonavir elevated the plasma concentration (C_{max} = 5.5 ± 2.0 μg/ml) and lead to sustained mean concentrations exceeding 0.1 μg/ml, even after 24 hours. Walmsley *et al*. (2002:2039) conducted a randomised, double-blind, multi-centre trial to compare the efficacy of lopinavir-ritonavir to that of nelfinavir on 653 HIV-infected patients who had not received antiviral therapy for more than 14 days. At week 24, 79 % of the patients treated with lopinavir-ritonavir and 71 % of the patients treated with nelfinavir had fewer than 400 copies of HIV RNA per millilitre ($P < 0.05$). At week 48, 67 % of patients treated with lopinavir-ritonavir and 52 % of patients treated with nelfinavir had fewer than 50 copies of HIV RNA per millilitre ($P < 0.001$). Discontinuation of treatment due to virologic failure occurred more frequently among patients receiving nelfinavir (9.2 %) than patients treated with lopinavir-ritonavir (0.6 %). The most common adverse effects were diarrhoea and nausea, while lipodystrophy or lipoatropy were also reported in 5 % of patients receiving lopinavir-ritonavir. One patient also developed lactic acidosis. Patient adherence was similar in all the treatment groups, and was found to be closely associated with treatment response. Patient adherence was 89 % for all those who showed a satisfactory response at week 48, while the adherence was only 61 % for those patients without a response at week 48 ($P < 0.001$). Walmsley *et al*. (2002:2045) concluded that the combination therapy of lopinavir-ritonavir demonstrated superior antiviral activity, high levels of tolerability and a high barrier to resistance, making it the ideal initial drug treatment for HIV infection.

The current dose of lopinavir-ritonavir is 400 mg lopinavir and 100 mg ritonavir, orally every 12 hours with food (a well known tactic to enhance the absorption of hydrophobic drugs like peptidomimetics). The adverse effects, namely diarrhoea and lipodystrophy, are consistent with those reported by Walmsley *et al*. (2002:2042). High levels of serum binding (98 – 99 %) means caution should be taken when prescribing other drugs that could displace lopinavir from serum proteins, or that could themselves be displaced by lopinavir-ritonavir (Rossiter, 2010:339).

At the time of this study, no polymorphism data had been reported on lopinavir in any peer reviewed scientific journals. Only one patent application, claiming to have identified lopinavir polymorphs, is available (Dickman *et al*., 2003). However, the data contained in the patent application is incomplete and unrefined, even after four revisions, and none of the interferograms or diffractograms corresponds to those presented in this study. Therefore, this study presents the first true physicochemical analysis and polymorphism screening of lopinavir.

The peptidomimetic structure of lopinavir is not only an important factor when it comes to dealing with the bioavailability of the drug, but it can also play an important role in its solid-state properties. Proteins (and peptides for that matter) are well known for their structural flexibility and their capacity to undergo large amounts of diverse molecular interactions. Looking again at the energy landscape (figure 3.2), it is clear that the amount of energy minima is determined by the amount of molecular coordination the system can adopt. Based on the size of the molecule, the amount of unhindered chiral points (four in this case), the abundance of hydrogen bond donors and acceptors and the possibility of π-π stacking, one might expect lopinavir to adopt several energy minima. This means that lopinavir can potentially form several polymorphs and that there is a high probability for lopinavir to form amorphous material. The extent to which these assumptions, based on the energy landscape, are true will be investigated in the coming sections.

6.2 MATERIALS

Lopinavir raw material (batch number AABH006954) was purchased from Dr. Reddy's Laboratories Ltd., Andhra Pradesh, India, as a fine off-white powder.

6.3 POLYMORPHISM STUDY

6.3.1 INITIAL POLYMORPH SCREENING

The same procedure described in section 5.3.1 for didanosine was followed here. Since no quantitative data concerning lopinavir's aqueous or organic solvent solubility is given in any pharmacopoeia or scientific article, a three solvent preliminary recrystallisation was attempted to ascertain which solvents could prove promising. The first three solvents used were ethanol (EtOH), ethyl acetate (EtOAc) and petroleum ether (PE), to cover a wide range of polarities. Lopinavir was freely soluble in EtOH, to such an extent that 10 g dissolved in

only 10 ml without the EtOH even reaching boiling point. After 2 years still no crystals formed in EtOH and, coupled with the large amounts of lopinavir used in the attempt, it was deemed impractical for recrystallisation. Lopinavir crystals formed over night from EtOAc, while lopinavir was insoluble in PE. Based on the findings from the preliminary recrystallisation, it was decided to investigate solvents with polarities close to that of EtOAc. A summary of the initial polymorph screening is given in table 6.2.

Table 6.2: The initial screening of lopinavir for crystal forming solvents

	Recrystallisation information		
Solvent	**ml solvent per 2 g lopinavir**	**Product formed?**	**Nature of product formed**
Acetone	20	Yes	Large plate-like crystals
Acetonitrile	Insoluble	No	
1-Butanol	Insoluble	No	
2-Butanol	Insoluble	No	
Chloroform	50	Yes	Highly viscous resin
Dichloromethane	40	Yes	Highly viscous resin
Diethyl ether	110	Yes	Fine flakes
Dimethylformamide	300	No	
Dimethylsulfoxide	200	No	
1,4-Dioxane	Insoluble	No	
Ethanol	< 1	No	
Ethyl Acetate	20	Yes	Long hexagonal crystals
Methanol	400	No	
1-Pentanol	Insoluble	No	
2-Pentanol	Insoluble	No	
Petroleum ether	Insoluble	No	
1-Propanol	1800	No	
2-Propanol	Insoluble	No	
Tetrahydrofuran	50	No	
Toluene	Insoluble	No	
Water	Insoluble	No	

However, recrystallisation from dichloromethane (DCM) and chloroform ($CHCl_3$) did not yield any crystals. Instead, a highly viscous gel formed on the bottom of the beaker, which

seemed to solidify upon standing but still retained its gum-like properties for several months. Since DCM and $CHCl_3$ only gave highly amorphous products, it was postulated that the formation of crystals was somehow dependent on the ester group of EtOAc. Unfortunately no other organic solvents containing esters were present in our laboratory, therefore, to test the hypothesis several other solvents with functional groups resembling segments of the ester functional group were selected, namely THF and diethyl ether to represent the ether bridge and acetone to represent the carbonyl oxygen. Diethyl ether yielded a fine, white flaky residue on the bottom of the beaker while THF did not yield any precipitate (even after 2 years). Large plate-like crystals formed from acetone, indicating that an interaction between lopinavir and the carbonyl oxygen from a solvent was necessary for the formation of large, single crystal quality crystals. The crystals obtained from acetone took up to several days longer to form than those obtained from EtOAc. Similar to EtOH and THF, no recrystallisation product was obtained from dimethylformamide (DMF), DMSO, methanol or 1-propanol. Unlike didanosine, the products obtained from the initial screening of lopinavir were structurally quite different, with visual differences in morphology and two obvious amorphous forms. The five products obtained were compared with the raw material and investigated further.

6.3.2 THERMAL ANALYSIS

6.3.2.1 LOPINAVIR RAW MATERIAL

Since the melting point of lopinavir is not reported in any of the official pharmacopoeias, DSC analysis was used in an attempt to determine it (figure 6.2). The initial DSC thermogram (red trace in figure 6.2) failed to give satisfactory information concerning lopinavir's solid-state thermal properties. The sharp enthalpy increase in the early stages of the run could be indicative of amorphous material, however, without a clear T_g such assumptions remained unproven. The peak at 347 K was too broad to be consistent with a melting peak, and was probably the result of multiple relaxations (arising from a wide distribution of molecular coordinations from across the energy landscape in figure 3.2) taking place around the same time as a result of cooperative molecular motions, yet again, these were just assumptions. A thermogram like this was simply not good enough to draw any scientific conclusions from. To investigate the possibility of the raw material being amorphous, it was annealed at 363 K for 10 minutes, cooled at 10 K per minute to 278 K and reheated at 10 K per minute to 450 K.

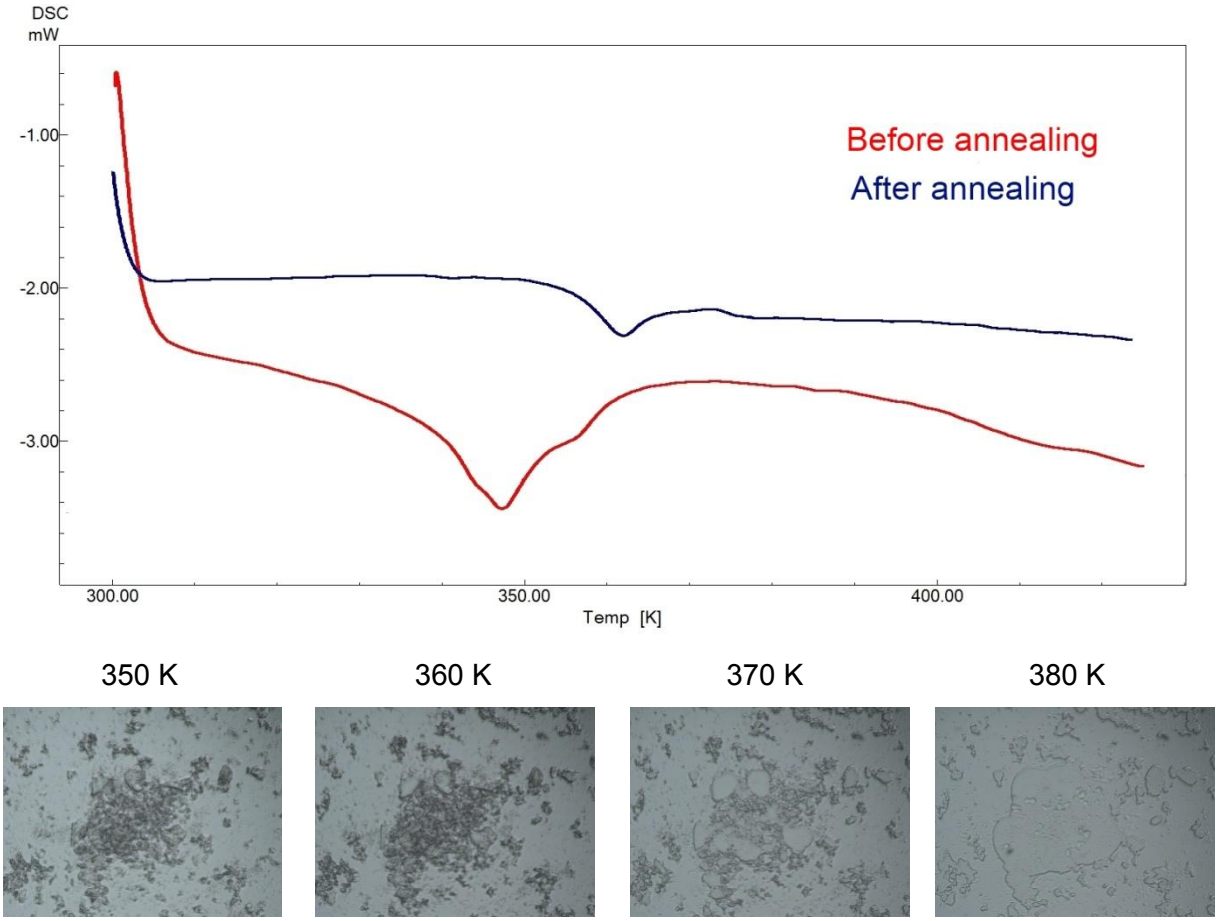

Figure 6.2: Thermal analysis of lopinavir raw material, including DSC thermograms and hot stage micrographs.

All of the DSC samples were run with a pierced lid. The resulting thermogram (blue trace in figure 6.2) gave a clear base line with a well defined T_g at 355 K. The system was also in a higher enthalpy state after the T_g, which is consistent with amorphous material above its T_g, and there was a small exothermic peak following the T_g, which is consistent with recrystallisation as a result of increased molecular motion. Between 370 and 380 K the system recovers enthalpy again and continues on an endothermic slope for the rest of the measurement, which is indicative of a material becoming more liquid. To visually corroborate the findings from the DSC, hot stage micrographs of the raw material were taken (figure 6.2). All the hot stage micrographs in this study were taken at a magnification of 100 x. There was a marked increase in the volume of the raw material granules above T_g (as seen when comparing the micrograph taken at 360 K to the one at 350 K), which is consistent with figure 3.3's depiction of an amorphous material's variation in volume with temperature.

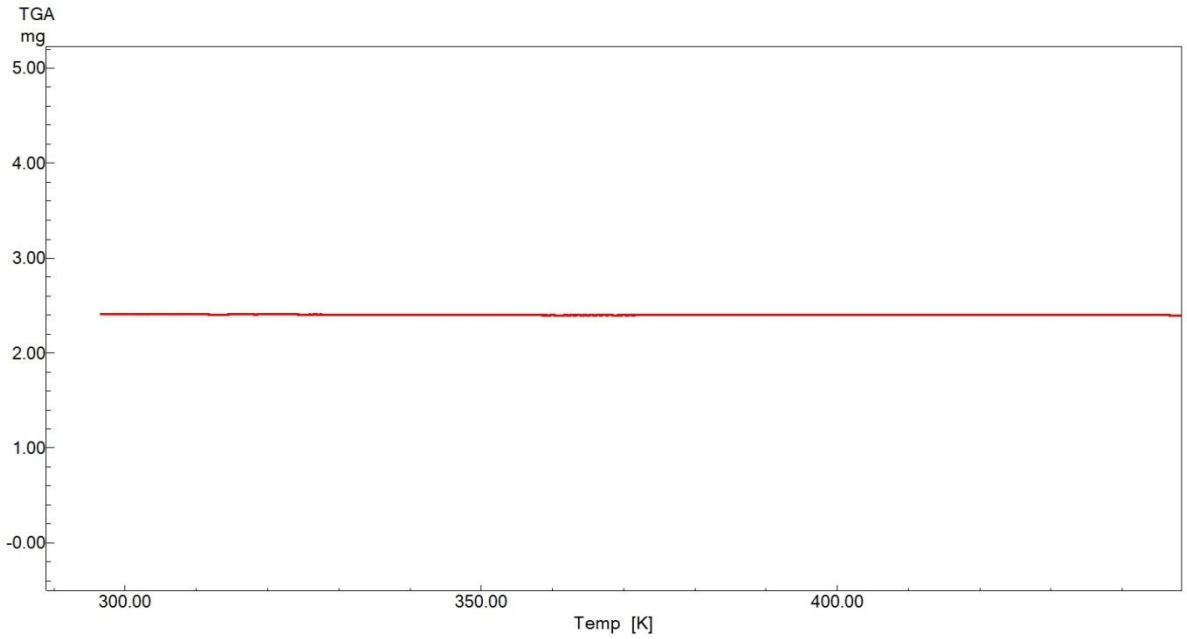

Figure 6.3: TGA of lopinavir raw material.

At 370 K, the temperature roughly corresponding to the exothermic peak on the DSC thermogram, lopinavir raw material appears to be melted, yet does not flow together, indicating that some form of anisotropy is keeping the system from melting altogether and becoming isotropic. This characteristic closely resembles thermotropic LC behaviour. From 380 K, the entire system melts and flows together. Although no evolution of volatiles from the raw material was visible on the micrographs, TGA was still performed to verify the absence of any entrapped or adsorbed liquid on the raw material (figure 6.3). The absence of any weight loss on the TGA indicates that the raw material does not contain any residual, or acquired, water or solvents. The thermal events seen on the DSC traces can therefore be reliably interpreted as glass transitions. Considering the origins and chemical structure of peptidomimetic drugs, it should come as little surprise that it exists in the amorphous state. It was decided to investigate the possibility of lopinavir retaining this amorphous character in other seemingly crystalline forms.

6.3.2.2 LOPINAVIR CRYSTALS FROM ETHYL ACETATE

As mentioned earlier, lopinavir recrystallised from ethyl acetate over night.

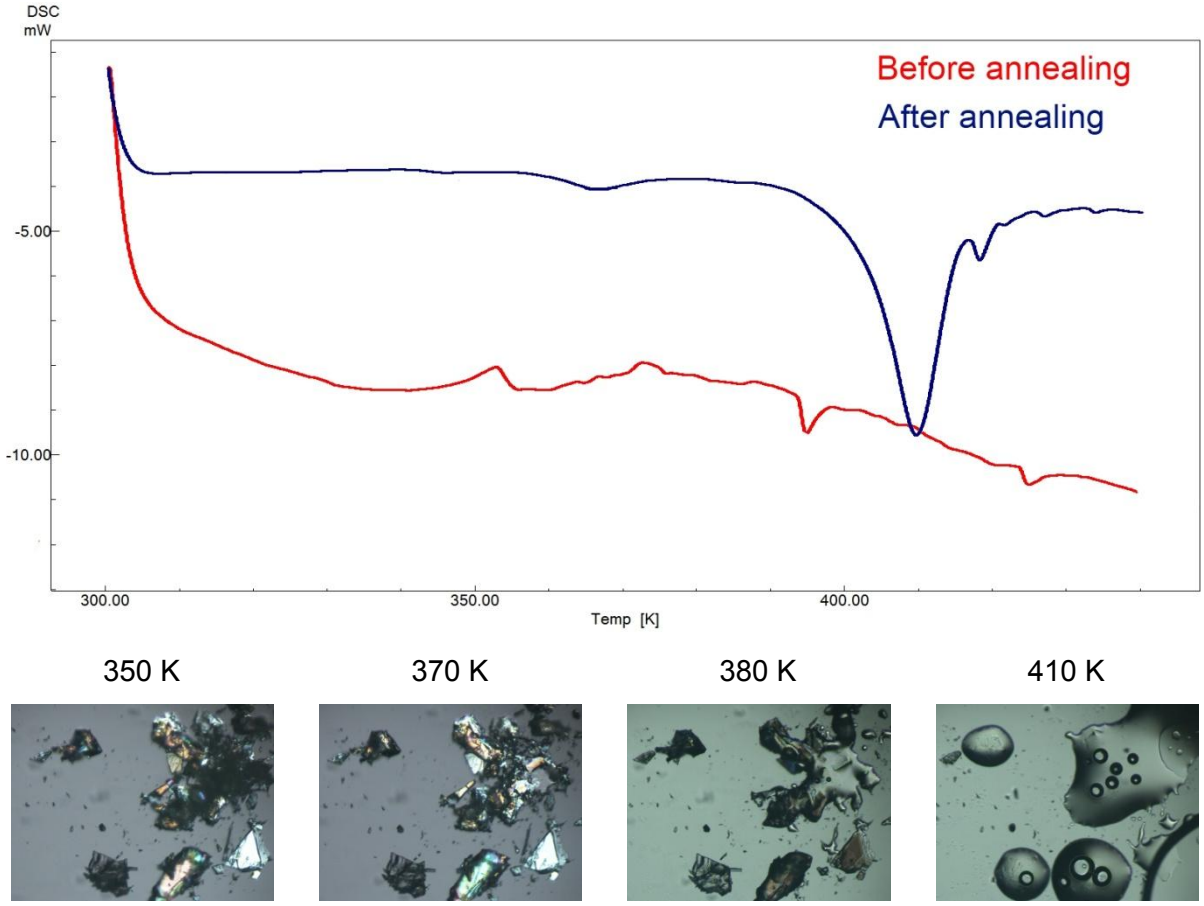

Figure 6.4: Thermal analysis of lopinavir recrystallised from ethyl acetate.

These crystals had a long, hexagonal morphology and grew out of a central point. DSC was used (figure 6.4), according to the method described for the raw material. The amount of detail lost if the sample is not annealed properly is extensive. After annealing, the T_g, small crystallisation exotherm and melting endotherm can be seen clearly. Hot stage micrographs show a clear increase in liquid-like properties of the crystals above T_g and, from the micrograph taken at 380 K it is clear that not all of the amorphous material crystallises at the crystallisation exotherm. Interestingly, there is a small endothermic peak preceding the T_g, which could probably be a β-relaxation (this will be investigated shortly). Another point of interest is the melting endotherm, which is much broader than endothermic peaks usually associated with melting. The shape is more consistent with desolvation peaks, and it was hypothesised that there could be ethyl acetate trapped so tightly in the crystal lattice that it is only evolved upon melting. Evidence from hot stage micrographs supports this theory, since some solvent evolution did take place at around 410 K, during melting of the crystals. To investigate this matter further, TGA was used (figure 6.5).

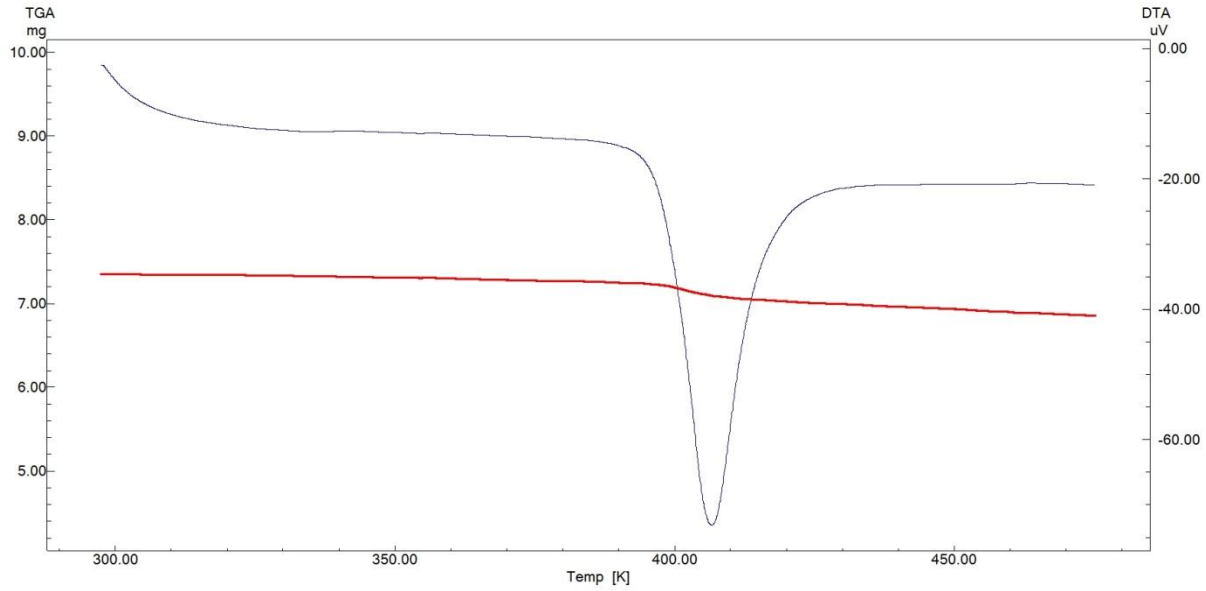

Figure 6.5: TGA of lopinavir recrystallised from ethyl acetate.

TGA of lopinavir recrystallised from ethyl acetate exhibited a 2.57 ± 0.45 % weight loss at a temperature corresponding to the melting temperature of the crystal. The ration for 1:1 solvent to drug stoichiometry is 12.3 %. This non-stoichiometric weight loss is most likely the result of disorder in the crystal system brought on by the amorphous content. Since crystalline regions are required to entrap the solvent molecules, amorphous fractions throughout the crystal can interfere with the periodicity of the crystal lattices and lead to non-stoichiometric solvent inclusion. The differential thermal analysis (DTA) trace (blue trace in figure 6.5) is incorporated in the background to better illustrate the coherence between the weight loss and the melting endotherm.

From the thermal analysis one can conclude that the crystals obtained from ethyl acetate are not only partially amorphous, but are also solvates. The fact that these crystals only desolvate upon melting, suggests that the solvent molecules are packed extremely tightly in the crystal lattice, and are not found in channels running through the crystals. This phenomenon will be investigated later on, by means of SXRD.

6.3.2.3 LOPINAVIR CRYSTALS FROM ACETONE

Lopinavir took several days longer to recrystallise from acetone, than it did from ethyl acetate. The crystals obtained from acetone were large, flat hexagonal plates. DSC and hot stage microscopy was used to investigate the thermal properties of these crystals.

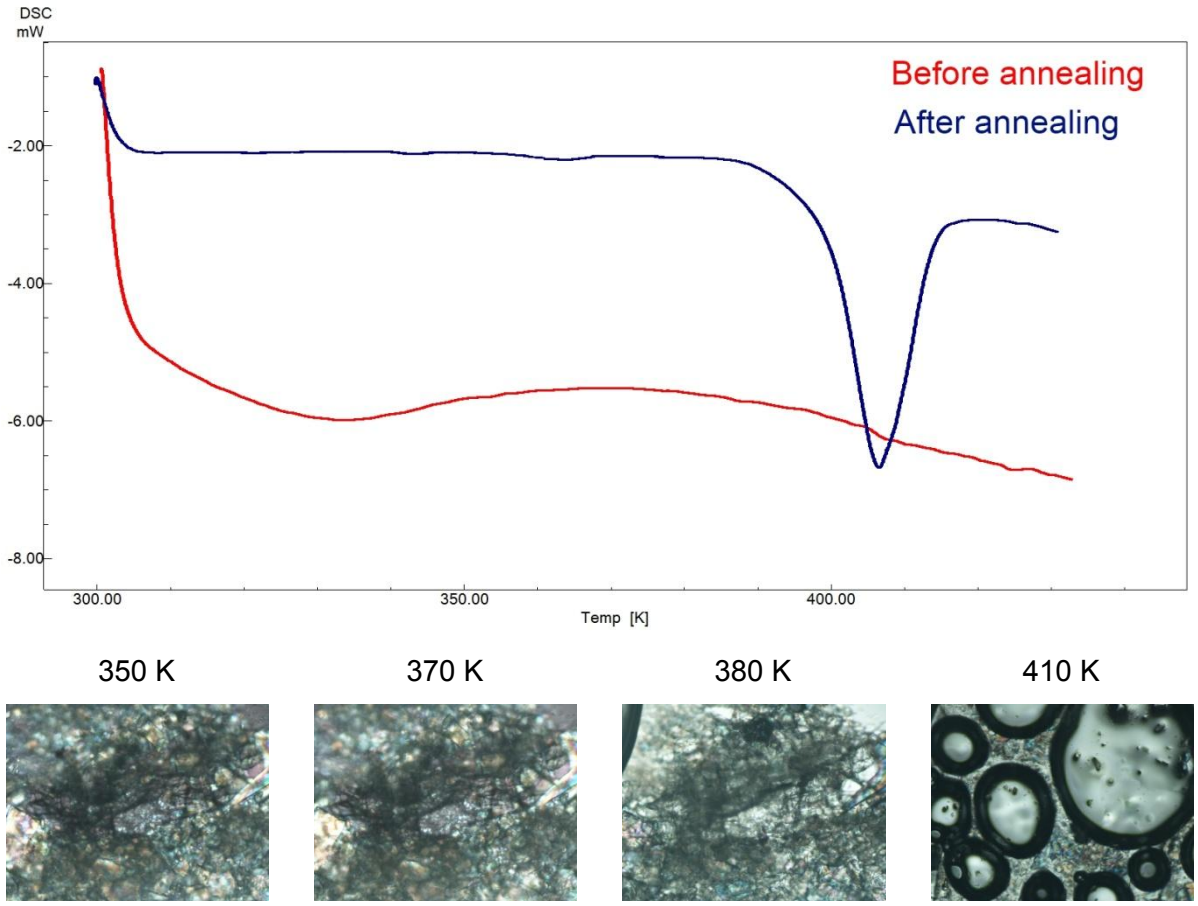

Figure 6.6: Thermal analysis of lopinavir recrystallised from acetone.

The thermogram of the lopinavir crystals obtained from acetone is almost identical to the thermogram obtained from the ethyl acetate crystals, including the broad melting endotherm. Although the multiple layers of plates, stacked on top of each other, made clear micrographs difficult to take, solvent evolution during crystal melting can clearly be seen. To corroborate these findings, TGA was employed (figure 6.7).

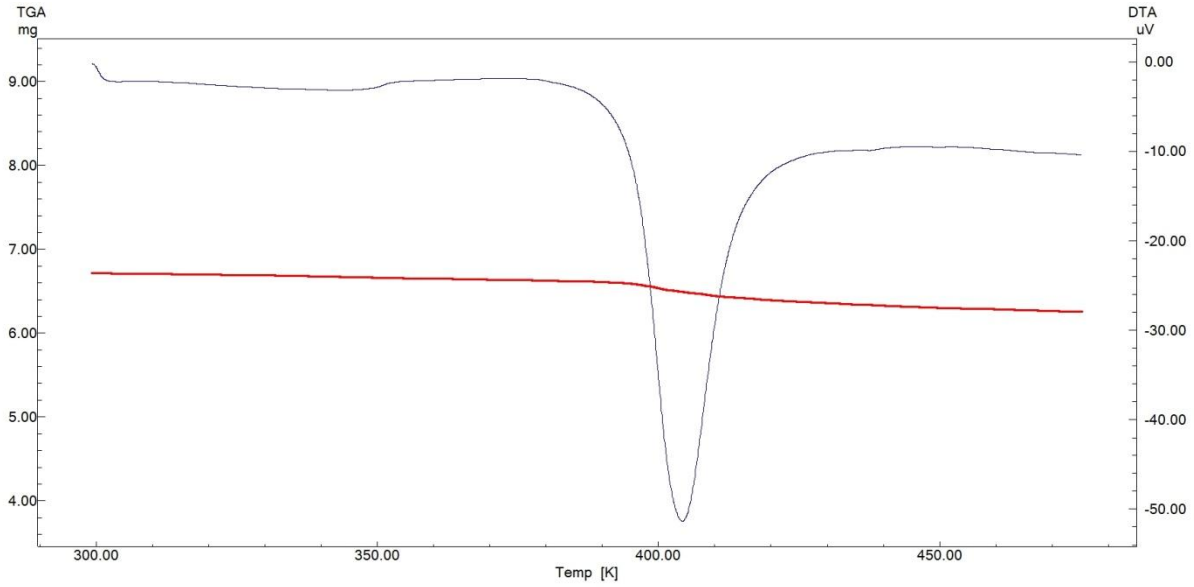

Figure 6.7: TGA of lopinavir recrystallised from acetone.

TGA of lopinavir recrystallised from acetone exhibited a 4.3 ± 0.21 % weight loss at the melting temperature. This indicates a stoichiometry of one acetone molecule for every two lopinavir molecules. Again, the DTA trace (blue) is included in the background to better illustrate the overlap in temperature between melting and desolvation.

From the thermal analysis of lopinavir crystals obtained from acetone, it is clear that these crystals are also partially amorphous and are also solvates. When comparing the macroscopic morphologic differences between the crystals obtained from acetone and ethyl acetate, both are hexagonal, but the crystals obtained from acetone are larger and flatter than those from ethyl acetate. Since the crystals took up to several days longer to form in acetone, the differences in morphology are consistent with the BFDH Law on the changes of the relative areas of crystal faces with regard to crystal growth rate. SXRD was employed to elucidate the differences in molecular packing between these crystals and also to investigate how the solvent molecules are entrapped in the crystal lattice. This data will be given later on in this chapter.

6.3.2.4 LOPINAVIR FLAKES FROM DIETHYL ETHER

The fine white flakes that precipitated from diethyl ether were macroscopically the recrystallisation product most similar to lopinavir raw material. These flakes were also studied using DSC and hot stage microscopy (figure 6.8), using the same methods as described for the raw material.

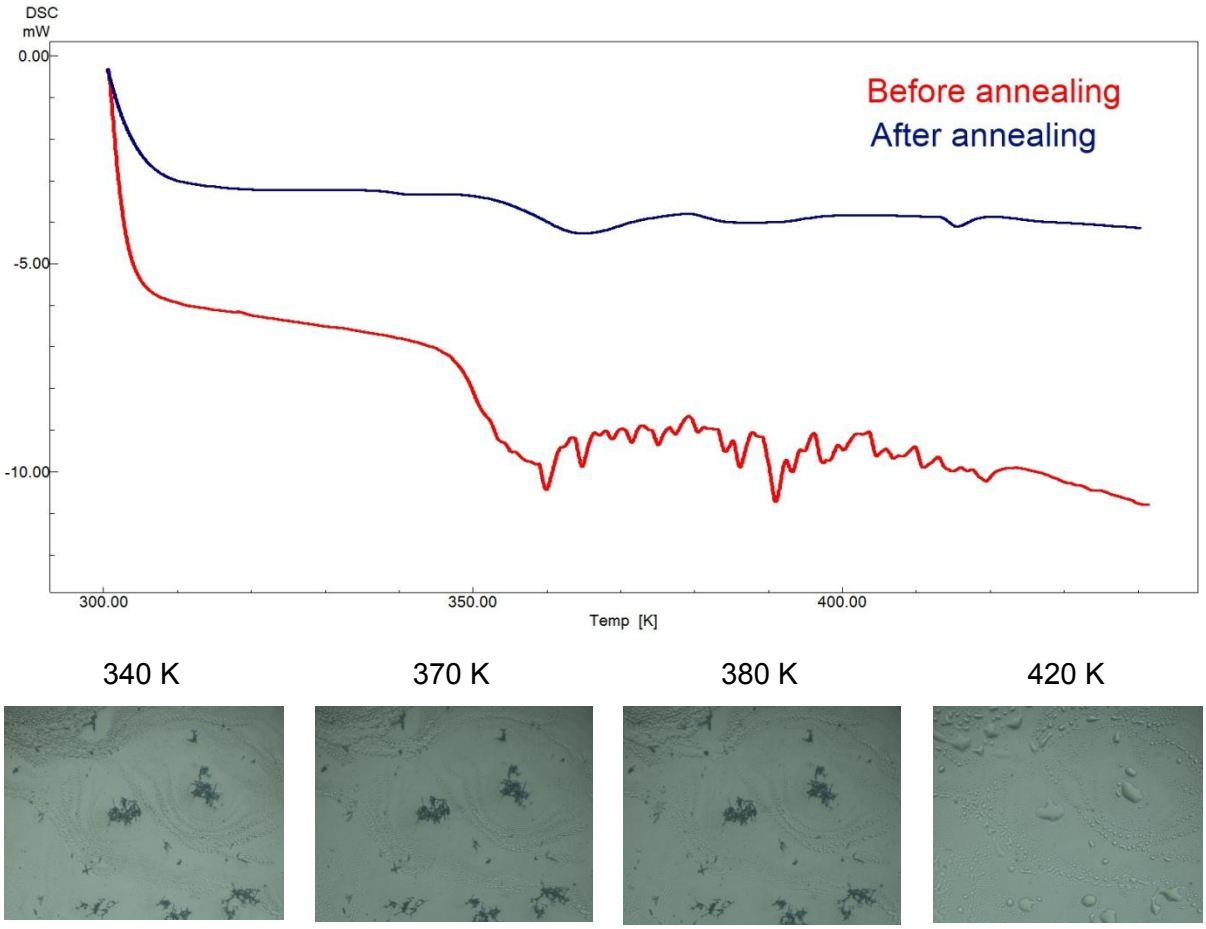

Figure 6.8: Thermal analysis of lopinavir recrystallised from diethyl ether.

The thermogram of an annealed sample shows a pronounced glass transition, crystallisation exotherm and small melting endotherm. When compared to the thermograms obtained from the recrystallisation products from ethyl acetate and acetone, a thermogram like this is consistent with a sample containing a larger amorphous fraction (figure 4.3). The hot stage micrographs are quite revealing. The recrystallisation product, that presents itself macroscopically as fine flakes, was in fact fine needle-shaped crystals surrounded by amorphous material. Above the T_g, there is a marked increase in volume, specifically of the amorphous fractions with a decrease in viscosity, as well as visual crystal growth from the amorphous material and small crystal "seeds" at 380 K (best seen in the upper left corner of the micrograph). To better visualise the crystal growth above T_g, enlargements of the upper left corners of the micrographs are given in figure 6.9.

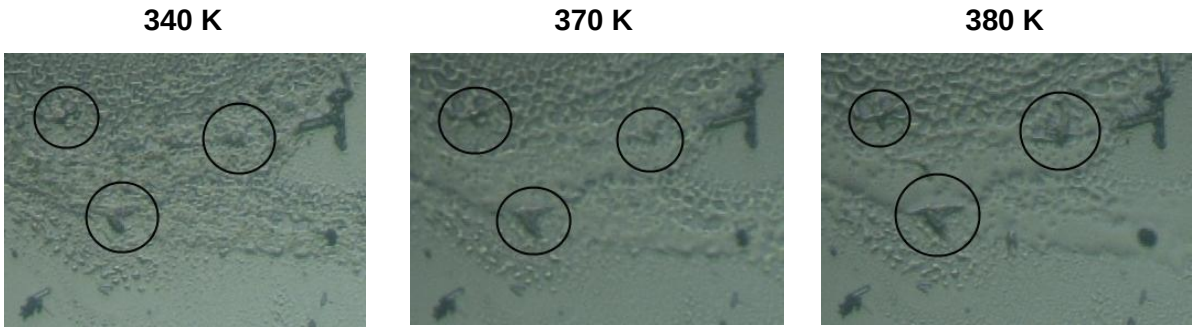

Figure 6.9: Enlargements of the micrographs in figure 6.8 to illustrate the changes taking place above T_g.

TGA was employed to determine the presence of any residual diethyl ether (figure 6.10).

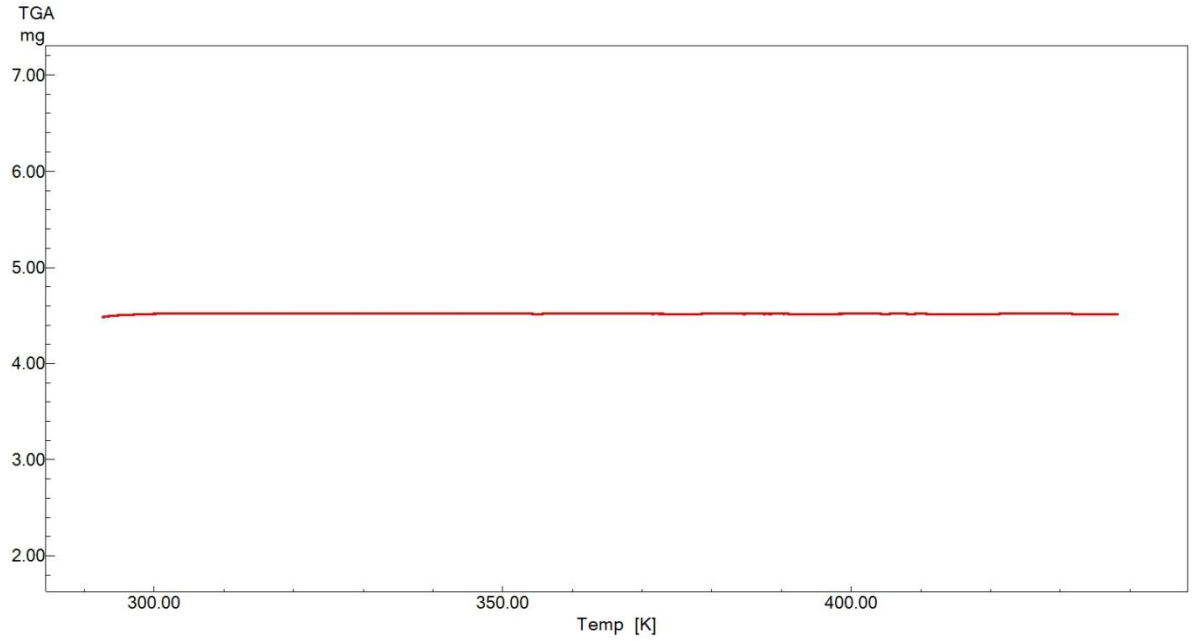

Figure 6.10: TGA of lopinavir recrystallised from diethyl ether.

The TGA shows no weight loss upon heating, indicating that the recrystallisation product from diethyl ether was not a solvate and that the sample tested was dry. The thermal events seen on the DSC can therefore be reliably interpreted as properties characteristic of amorphous material. The small melting endotherm is indicative of a small amount of crystalline content. From the hot stage micrographs the crystalline fraction can be seen imbedded in the amorphous material, and although the crystals might appear to be numerous, one should always remember that per volume unit, amorphous material weigh more than crystals because the molecules are more disorganised and are closer to each

other. The amorphous content might very well comprise the larger part of the sample weight. The amorphous content in each of the recrystallisation products will be determined later on in this chapter.

6.3.2.5 LOPINAVIR RESIN FROM CHLOROFORM

With all the crystalline recrystallisation products analysed, the focus was shifted to the more obvious amorphous recrystallisation products. The first was the resin obtained from chloroform. As mentioned earlier, this resin seemed to solidify upon standing, however, it retained some of its gum-like properties for several months. DSC and hot stage microscopy was used to investigate, according to the method described for the raw material (figure 6.11).

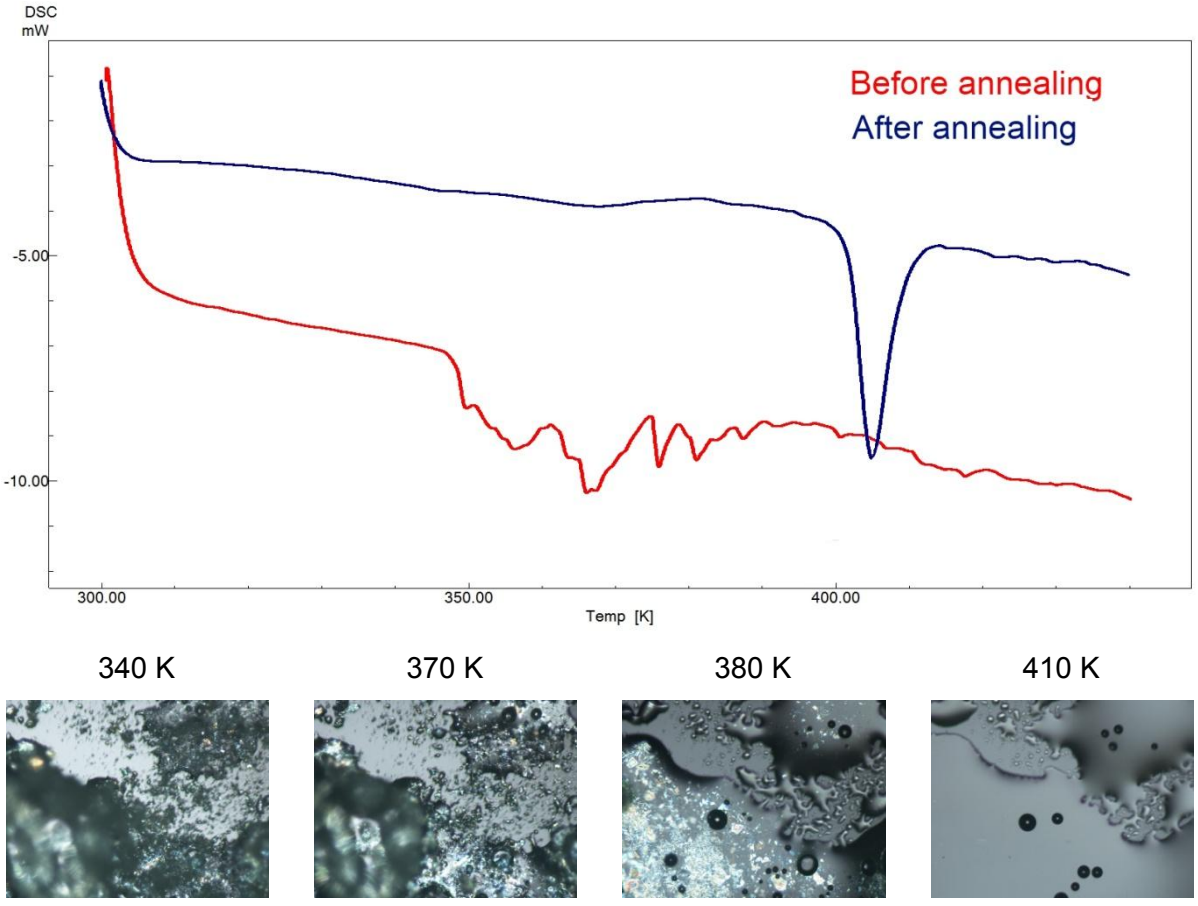

Figure 6.11: Thermal analysis of the lopinavir resin obtained from chloroform.

Interestingly, the thermogram obtained from the lopinavir resin resembles that of a sample containing a large amount of crystalline material. This can be deduced, not only from the shallow glass transition, but also from the relatively large melting endotherm when compared

to the DSC thermogram of the needles obtained from diethyl ether. The hot stage micrographs once again proved invaluable in elucidating the thermal events seen on the DSC thermogram. Just above the T_g, there is a clear increase in liquid-like behaviour of the lopinavir resin. At 380 K, the temperature corresponding to the crystallisation exotherm on the DSC, large amounts of crystals (anisotropic) can be seen in the melt (isotropic). This corresponds with similar behaviour exhibited by the previous recrystallisation products. The large melting endotherm on the DSC thermogram indicates that there was a large amount of crystalline content in the resin from the beginning (Van den Mooter *et al*., 2001:263). To confirm this, micrographs were taken of the resin at room temperature (figure 6.12). Micrographs A and B were taken at the exact same adjustment and temperature, the only difference was that for micrograph B the polarised light filter was turned through 90°. This filters out all the isotropic material and gives better resolution of anisotropic crystalline material. The result shows that, embedded in the seemingly amorphous resin (apart from the larger crystals visible in micrograph A), there are numerous small crystals scattered throughout the sample. The amorphous content will be calculated later on in this chapter.

A B

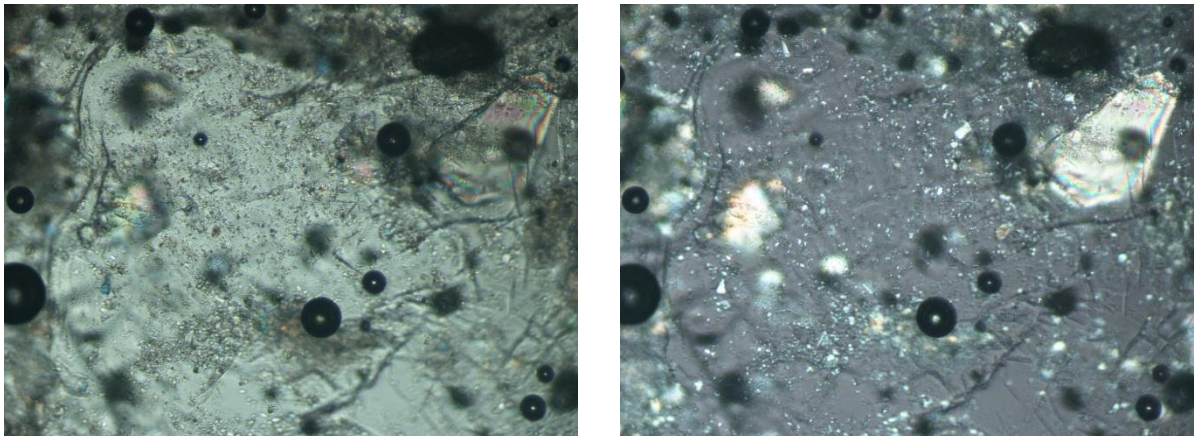

Figure 6.12: Hot stage micrographs of lopinavir resin from chloroform.

Some bubbles can be seen in the micrographs and, although the melting endotherm on the DSC thermogram was not as broad as that of the solvates described above, TGA was employed to determine the presence of any residual chloroform (figure 6.13).

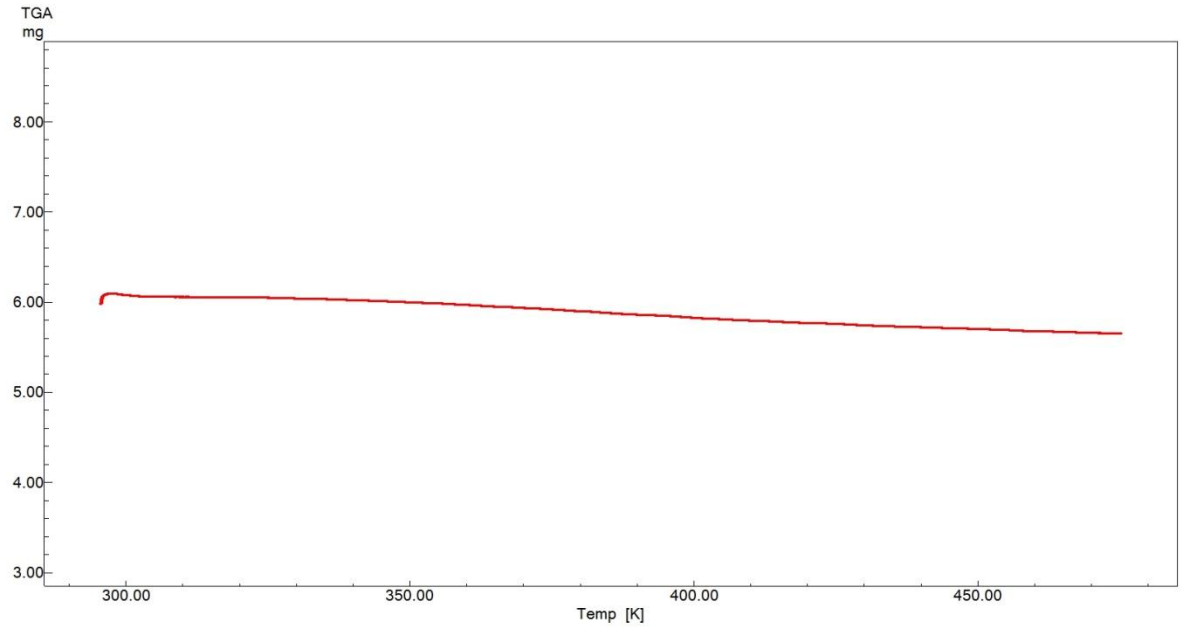

Figure 6.13: TGA analysis of lopinavir resin obtained from chloroform.

There is indeed weight loss on the TGA, indicating the presence of residual chloroform. However, there is no clear base line from which to measure the weight loss. The weight loss starts upon heating and continues on an almost constant slope all the way through. This is consistent with solvent loss from the surface of material, unlike the TGA's of the recrystallisation products from ethyl acetate and acetone (figures 6.5 and 6.7 respectively). Another indicator that the residual chloroform is not entrapped within the resin is the DSC thermogram's melting endotherm, which is not broad enough to be consistent with desolvation. Chloroform present on the surface of the resin should have no effect on the DSC analysis from figure 6.11, because it will be lost during the annealing stage. The thermogram in figure 6.11 was therefore taken as a reliable indicator of the thermodynamic properties of the lopinavir resin obtained from chloroform.

6.3.2.6 LOPINAVIR RESIN FROM DICHLOROMETHANE

Macroscopically, there was no difference between the resins obtained from dichloromethane and chloroform. Thermal analysis of the resin from chloroform has shown it to contain large amounts of crystalline material. DSC and hot stage microscopy was used to investigate the resin obtained from dichloromethane (figure 6.14).

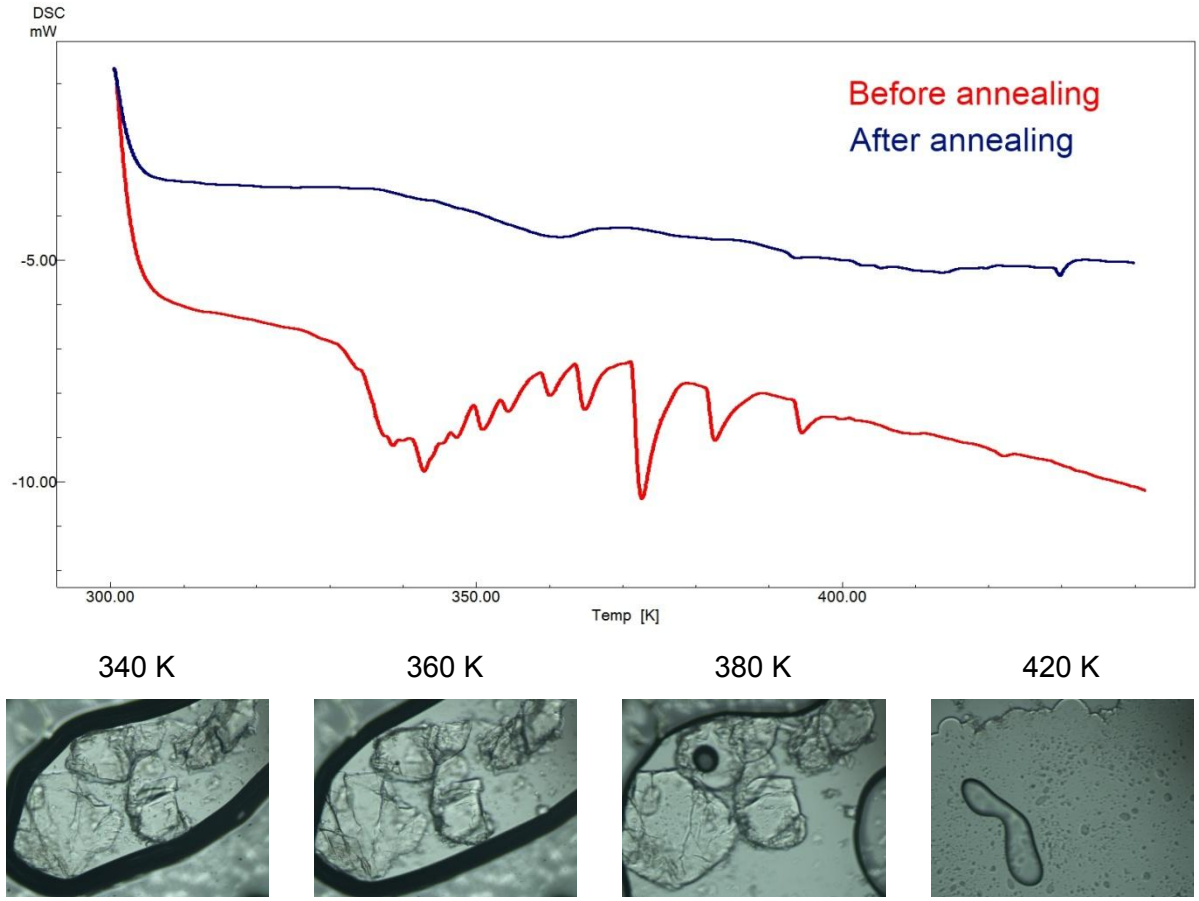

Figure 6.14: Thermal analysis of lopinavir resin from dichloromethane.

The DSC thermogram of the resin obtained from dichloromethane is quite different from the one of the resin obtained from chloroform. The thermogram in figure 6.14 has more in common with the thermograms of the raw material (figure 6.2) and the fine needles obtained from diethyl ether (figure 6.8). The very small melting endotherm(s) makes reliable determination of this resin's melting point nearly impossible and is consistent with a material containing mostly amorphous material. The same trend is seen in figure 6.2 and also, to a lesser extent, in figure 6.8. The resin obtained from dichloromethane differs from the chloroform resin in the fact that it mainly consists of amorphous lopinavir. Hot stage micrographs were also more consistent with those obtained from the raw material than any of the other recrystallisation products.

To determine the presence of any residual dichloromethane in the resin, TGA was employed (figure 6.15).

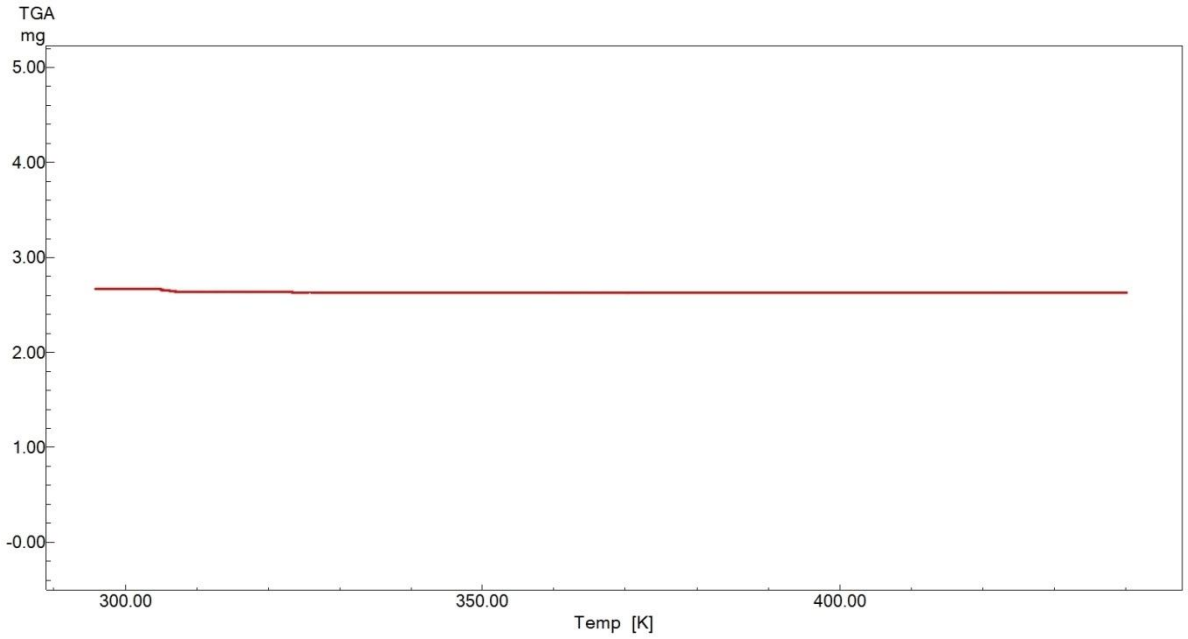

Figure 6.15: TGA of lopinavir resin from dichloromethane.

Apart from a small percentage of weight loss at the beginning of the run, most probably due to surface solvent loss, there is no weight loss during heating. This is consistent with the absence of solvent evolution from the resin during hot stage microscopy as well as the absence of a desolvation endotherm on the DSC thermogram.

Based on the thermal analysis, the lopinavir resin obtained from dichloromethane is the recrystallisation product which most resembles the raw material. This observation will be investigated further in the coming sections.

6.3.2.7 LOPINAVIR GLASS FROM QUENCH COOLING

Because lopinavir raw material and all of its recrystallisation products proved to be amorphous (at least to some extent), it was decided to create a lopinavir glass, to serve as a reference representing a 100 % amorphous form. Although one might argue that the raw material, being seemingly fully amorphous, can serve this purpose, the rationale behind the glass was that it would be prepared by the procedure normally used in the literature to prepare glasses. Lopinavir raw material was melted and the melt was immediately quenched with liquid nitrogen. This quenching of the melt “freezes” the molecules in the high entropy state in which they existed whilst in the liquid-state, thereby denying them the opportunity of arranging into energy minima and effectively yielding the optimal glass for the specific sample. The melt was quenched in liquid nitrogen until no further bubbles were evolved from the system and no further crackling noises could be heard, indicating that the entire system was the same temperature as the liquid nitrogen. The glass hereby obtained was

immediately analysed by means of DSC and hot stage microscopy (figure 6.16) according to the method described for the raw material.

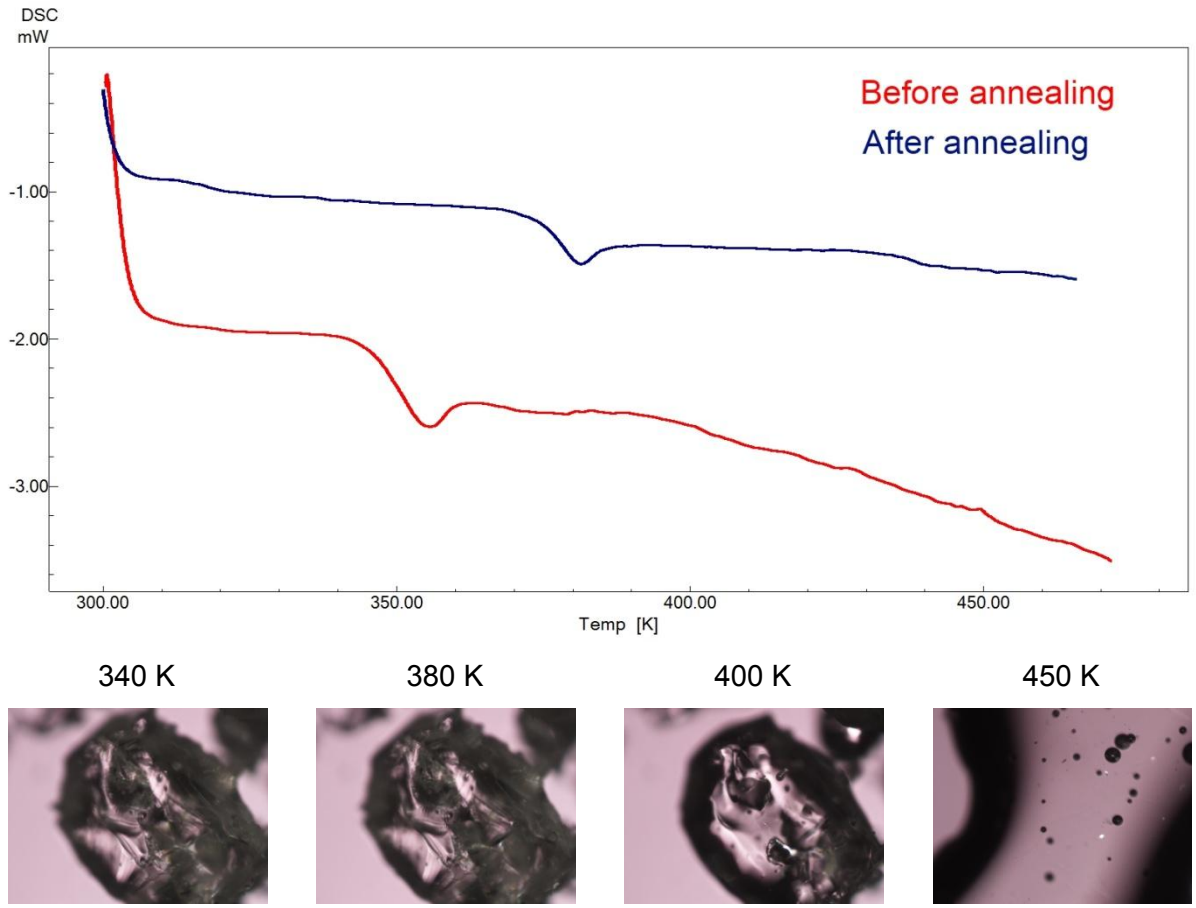

Figure 6.16: Thermal analysis of lopinavir glass from quench cooling.

As expected, the DSC thermogram of the sample before annealing does not show the same thermal chaos and does in fact show a clear glass transition. The reason being, that quenching of the melt is nothing more than a form of passive annealing. However, to further optimise the energy landscape in the glass, and to ensure its comparability with the other samples, it was annealed according to the method described for the raw material. The thermogram obtained (blue trace in figure 6.16) shows a marked increase in T_g, a trait consistent with that of all the annealed samples described previously and, a thermal phenomenon consistent with that of sample that now has a more homogeneous dispersion of molecular motions and a lower potential energy. Microscopically, the quench cooled glass has the appearance of shattered glass, and the thermal behaviour on the hot stage micrographs is consistent with that previously described for the other recrystallisation products and raw material.

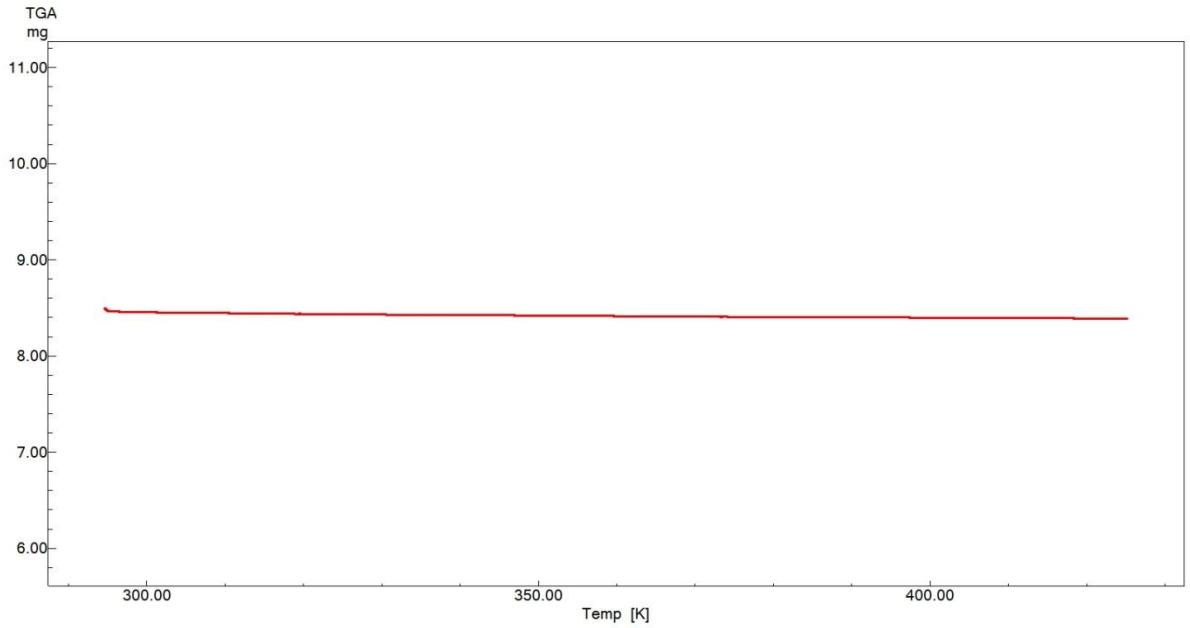

Figure 6.17: TGA of lopinavir glass obtained from quench cooling.

TGA of the lopinavir glass (figure 6.17) shows a slight drift in the base line. This drift is possibly the result of residual nitrogen evaporation from the surface of the glass, since the sample was analysed immediately after quenching.

The position of the T_g on the annealed DSC thermogram indicates a highly stable glass. Coupled with the high molecular entropy obtained from quench cooling the melt, this glass is indeed representative of the most stable lopinavir glass. In the coming sections, the other lopinavir samples will be compared to this glass as additional physicochemical properties are investigated.

6.3.2.8 LOPINAVIR GLASS FROM SLOW COOLING

Since all of the recrystallisation products formed at ambient temperature, it was decided to prepare a glass by cooling the melt under ambient temperature. Lopinavir raw material was melted, the melt was removed from the heating mantle and allowed to cool under ambient temperature. To test whether the melt had solidified throughout, the glass was loosened at one end with a spatula. If the entire glass came loose and could be removed without disturbing (cracking or chipping) any part of it, it was considered solidified and used for analysis. Although this method of preparing a glass is often used, it will not yield a glass as thermodynamically stable as its quench cooled counterpart. The molecules have a longer time scale in which to rearrange themselves into different energy minima, giving a more heterogeneous dispersion of densities and molecular mobility throughout the glass. One would expect a glass formed under these conditions to be highly metastable, and much

more susceptible to thermal and mechanical stresses. To investigate the thermal properties, DSC and hot stage microscopy was employed, using the method as described for the raw material (figure 6.18). Please note that, although cooled at ambient temperature, this glass will be referred to as slowly cooled for the rest of this study, simply to better differentiate between it and the quench cooled glass.

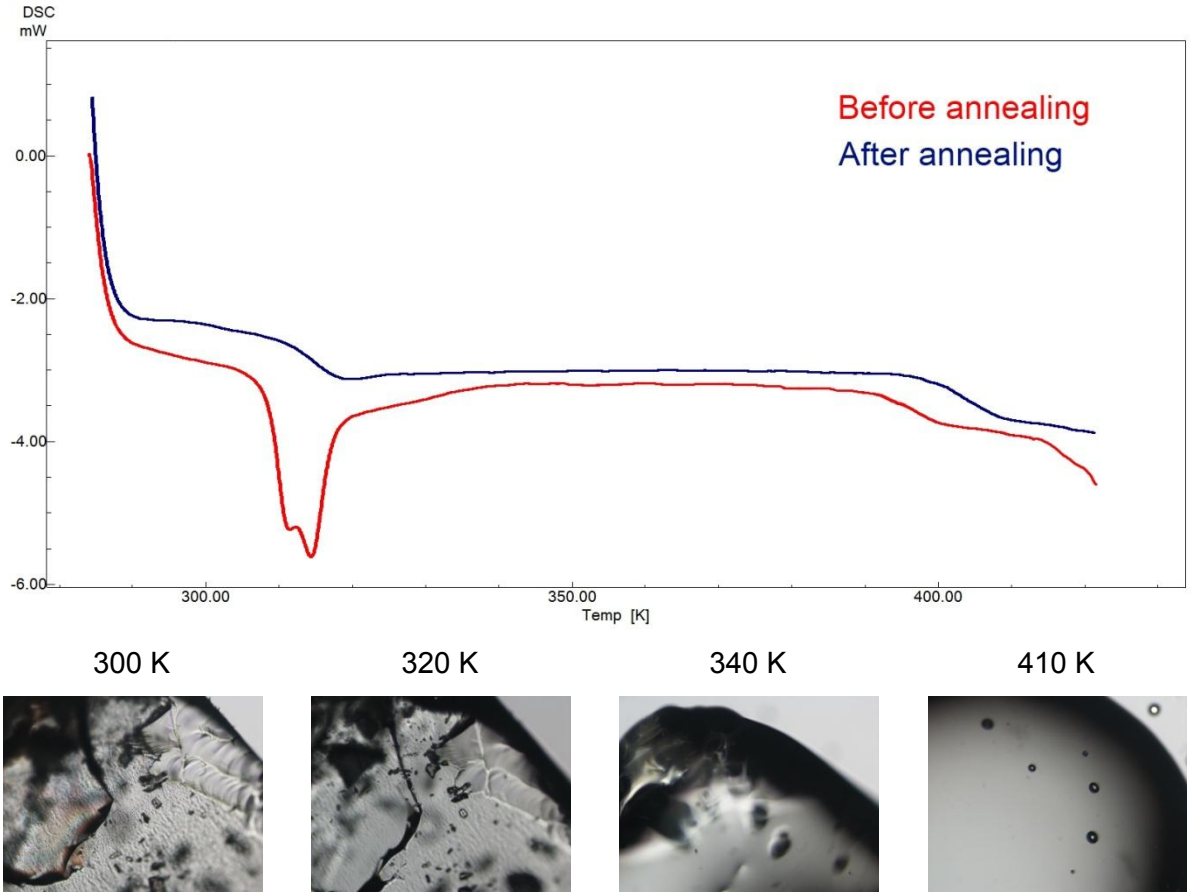

Figure 6.18: Thermal analysis of lopinavir glass from slow cooling.

From the DSC thermogram the first indications of this glass' instability becomes evident. The T_g corresponds to a temperature where the previously described samples and raw material were still at their respective base lines. From the micrographs, one can clearly see tiny ripples on the surface of the glass, a direct result of its heterogeneous composition.

To determine if the glass had absorbed or adsorbed any moisture, TGA was employed (figure 6.19). The TGA was negative for any weight loss, indicating that the lopinavir glass was dry. This is consistent with the hot stage micrographs which did not show any evolution of volatiles during heating.

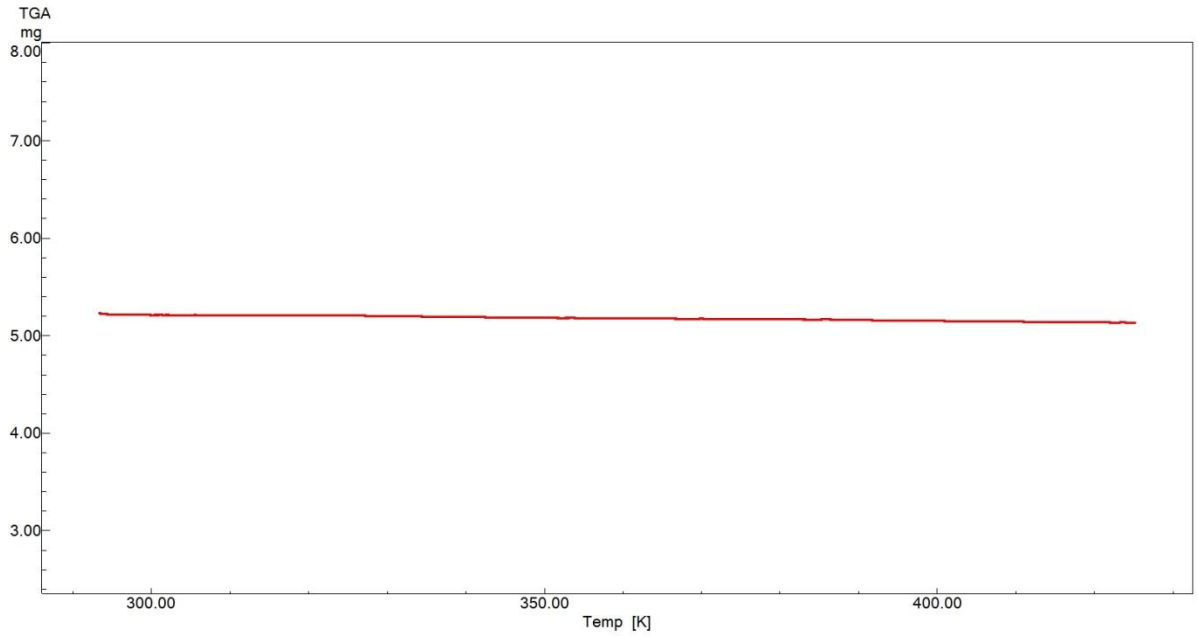

Figure 6.19: TGA of lopinavir glass obtained from slow cooling of the melt.

The lopinavir glass obtained from cooling at ambient temperature displays thermal behaviour consistent with that expected from a glass that was prepared at a slower cooling rate than its quench cooled counterpart. It also serves as an additional reference for the recrystallisation products, since it was prepared under relatively the same thermal conditions. The metastability of this glass is already evident in its very low T_g, and will be investigated further in the coming sections.

6.3.3 PXRD ANALYSIS

From the thermal analyses, we can deduce that lopinavir raw material is amorphous, and that the resin obtained from dichloromethane closely resembles the raw material as far as their thermal behaviour is concerned. The glasses obtained from the melt are also amorphous, with the glass obtained from quench cooling being far more thermodynamically stable than the glass obtained from cooling at ambient temperature.

Although amorphous materials are known to give diffuse halo bands on a PXRD diffractogram, the relative intensities of these halos can still give valuable information concerning the composition of the system. The intensities should still be subject to the electron density in the sample, as described in chapter 4. Therefore, the quench cooled glass, with its molecular packing being similar to that of a liquid (isotropic) but with the molecules much closer together because of the sharp decrease in volume brought on by the quenching, could be expected to display high intensity (counts), while the opposite would be true for the glass cooled at ambient temperature. To investigate this, an overlay of

equimolar amounts from all the amorphous material found and prepared in this study is presented here in figure 6.20.

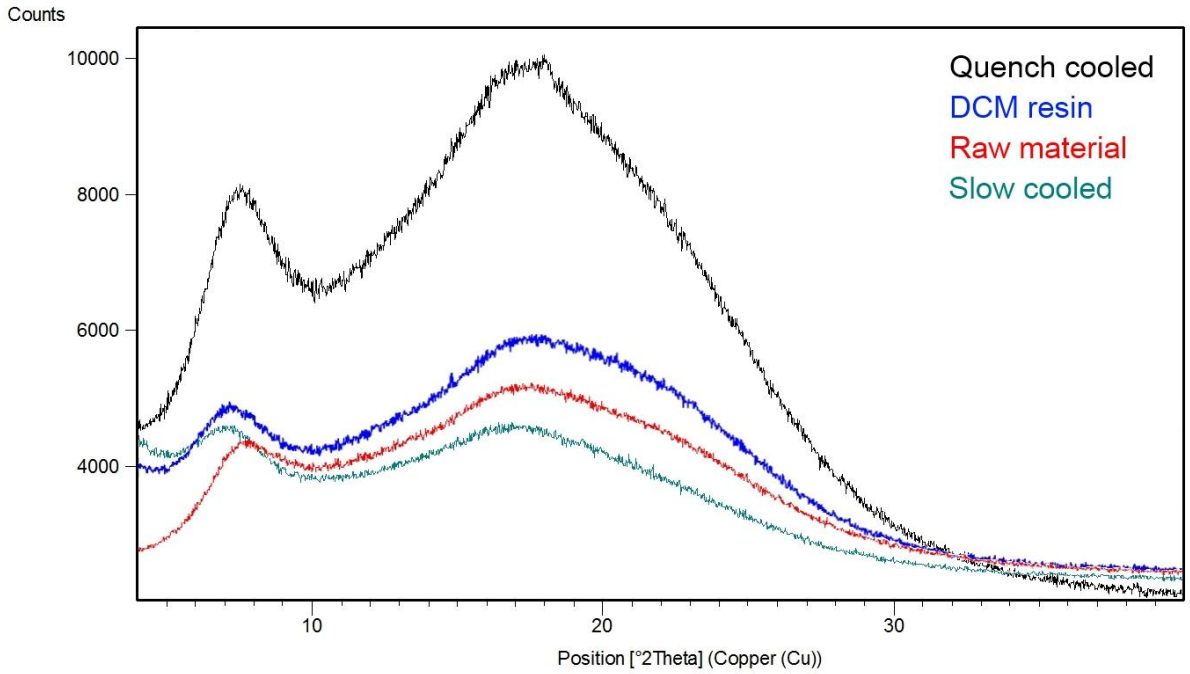

Figure 6.20: PXRD analysis of lopinavir raw material and its amorphous products.

The PXRD data are in excellent coherence with the thermal analyses reported earlier. Based on the T_g values of each sample, the PXRD data are consistent with regards to the stability of the quench cooled melt as well as the metastability of the slowly cooled melt. Although the PXRD diffractograms are consistent with what one would expect when looking at the thermal behaviour of each sample, it is always better to confirm an observation with more than one independent method. The thermodynamic differences between quench cooled and slow cooled melts will be thoroughly investigated as this chapter progresses.

Concerning the crystals obtained from ethyl acetate and acetone, the DSC thermograms show large melting endotherms. TGA has proven both crystals to be solvates which desolvate upon melting. PXRD diffractograms (figure 6.21) of these two crystals also show them both to be crystalline. The intensities of the peaks between °2θ values of 7 and 8 suggest that the crystals obtained from ethyl acetate are the more crystalline of the two. However, in the coming section on the degree of crystallinity a full spectrum approach will be used to investigate this. The diffractograms show clear differences in the positions of the peaks, indicating that the two crystals are indeed polymorphs.

Lopinavir crystals from ethyl acetate

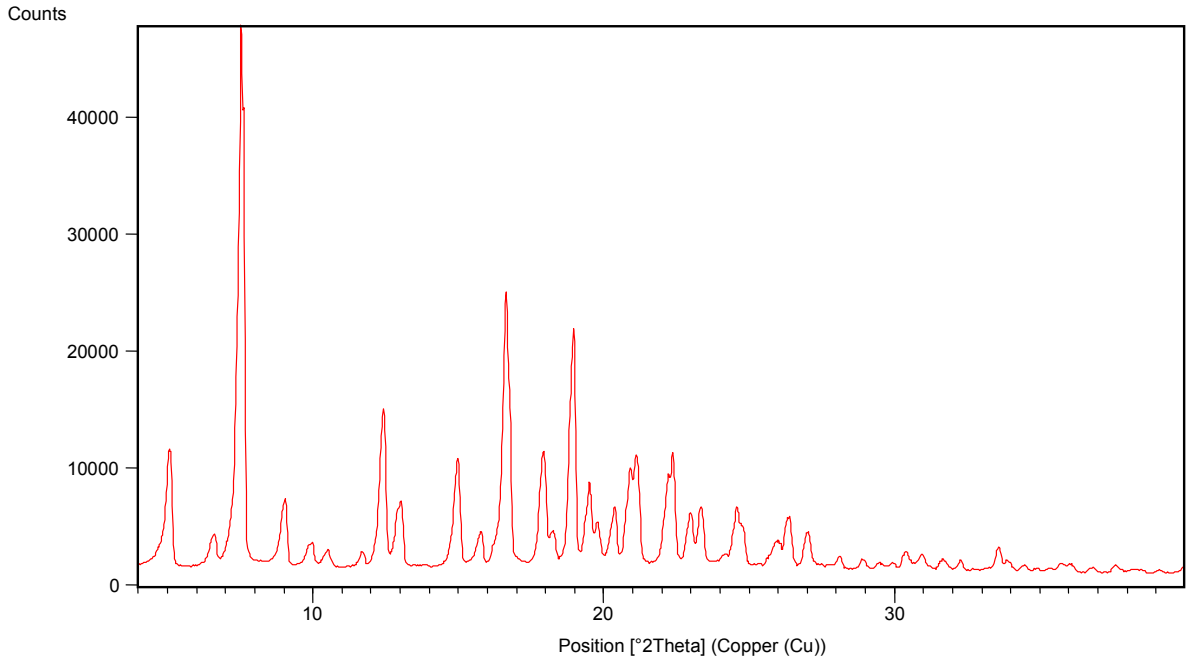

Lopinavir crystals from acetone

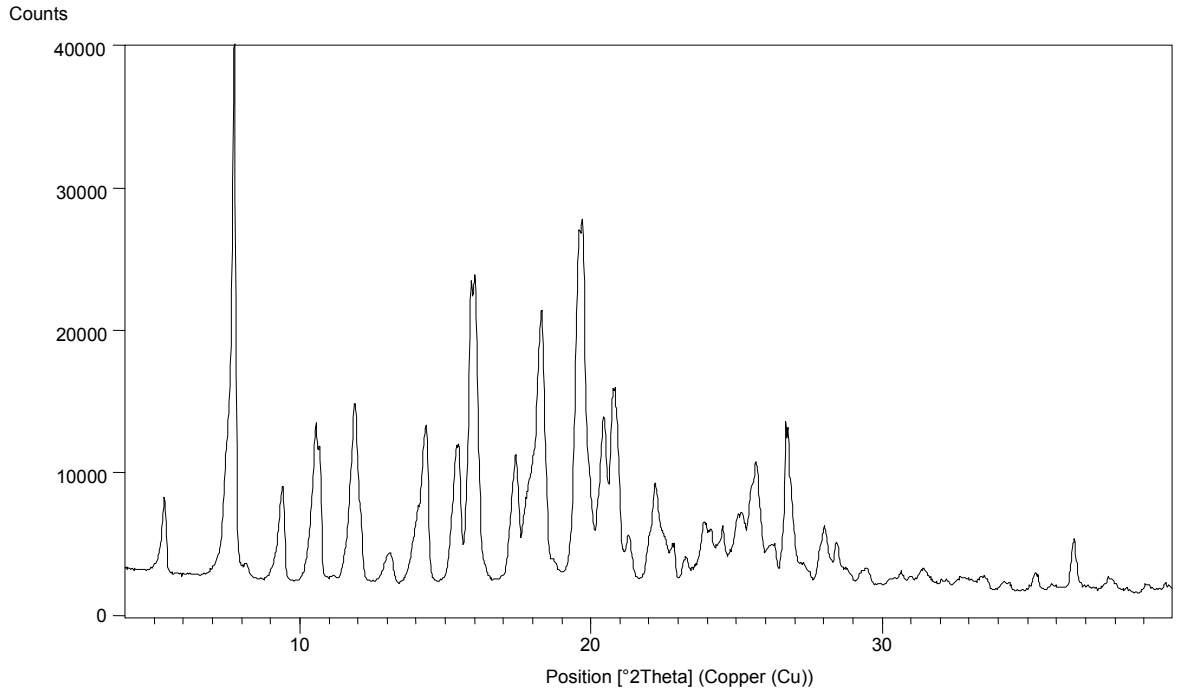

Figure 6.21: PXRD diffractograms of lopinavir crystals obtained from ethyl acetate and acetone.

The diffractograms of the lopinavir needles obtained from diethyl ether and the resin obtained from chloroform are given in figure 6.22.

Lopinavir needles from diethyl ether

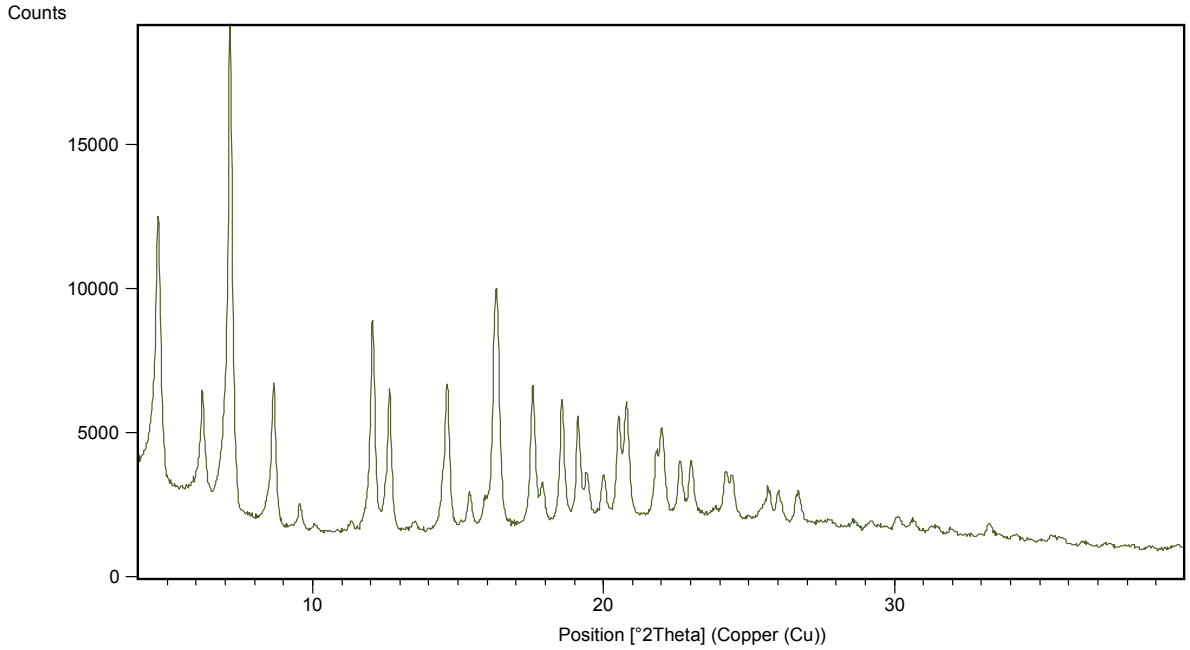

Lopinavir resin from chloroform

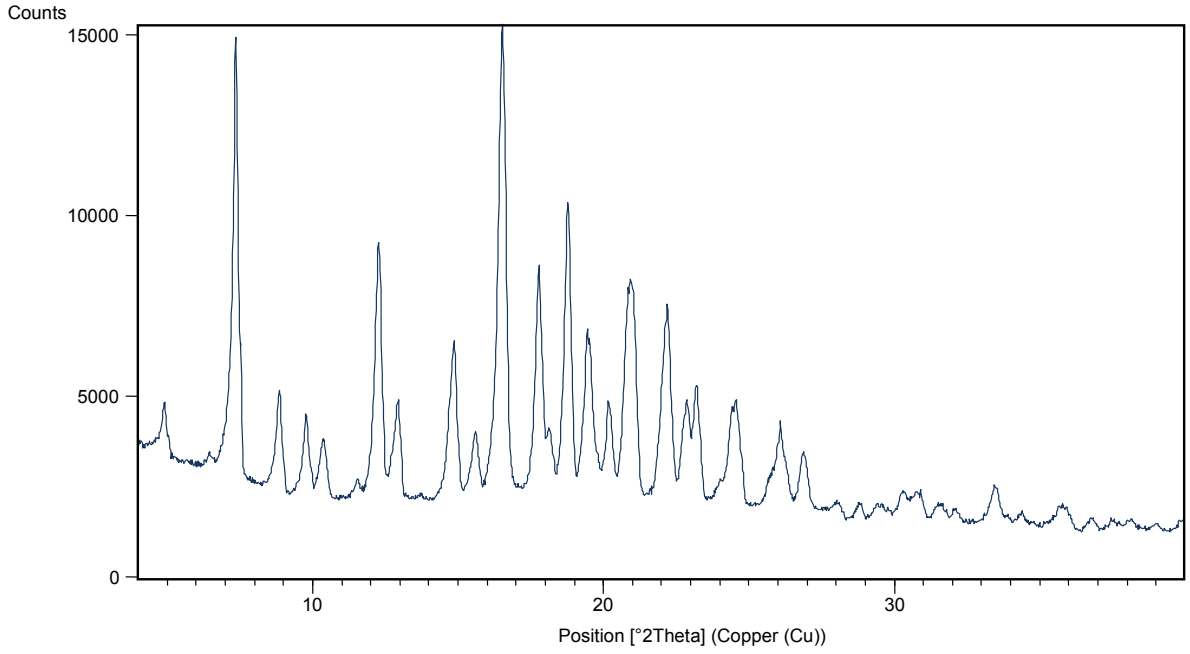

Figure 6.22: PXRD diffractograms of lopinavir needles from diethyl ether and lopinavir resin from chloroform.

The diffractograms not only show lower counts, but also the remnants of the diffuse halo in the base line, indicating that these recrystallisation products are not as crystalline as the crystals obtained from ethyl acetate and acetone and also that they contain varying amounts of amorphous lopinavir. The PXRD data of the lopinavir needles and resin are consistent

with their respective thermal analyses, which not only showed them to have glass transitions, but also melting endotherms several orders of magnitude smaller than those of the crystals. This is consistent with a sample that had only a small amount of crystalline content and more amorphous content than its crystalline counterpart.

The positions of the peaks on the diffractograms of the lopinavir needles and resin from chloroform not only differ from one another, but also from those of the crystals obtained from ethyl acetate and acetone, indicating that all four “crystalline” recrystallisation products are polymorphs of lopinavir. The exceptionally high counts of the diffuse halo obtained from the quench cooled lopinavir glass, compared to the rest of the amorphous lopinavir samples, reinforce its position as the ideal lopinavir glass. The quench cooled glass can therefore be reliably used as reference for the 100 % amorphous sample in the coming sections.

6.3.4 FTIR ANALYSIS

For the purpose of later using the FTIR data in determining the crystalline content of the lopinavir raw material, glasses and recrystallisation products, the y-axis of the interferograms (figures 6.23 to 6.24) are given in units of absorbance rather than transmission. In keeping with the Beer-Lambert Law when working with absorbance, the concentrations of all the samples analysed were kept constant (table 6.3), to ensure comparability. The mean values and standard deviations were obtained from 3 independent batches each analysed in triplicate.

Table 6.3: Concentrations of lopinavir samples used in the FTIR analysis

Sample	Mass of sample / 100 mg KBr (mg)
Raw material	5.7 ± 1.1
Ethyl acetate	5.8 ± 0.83
Acetone	4.3 ± 0.27
Diethyl ether	5.5 ± 0.81
Chloroform	6.2 ± 0.66
Dichloromethane	5.9 ± 0.81
Slow cooled	5.4 ± 0.94
Quench cooled	5.6 ± 0.88

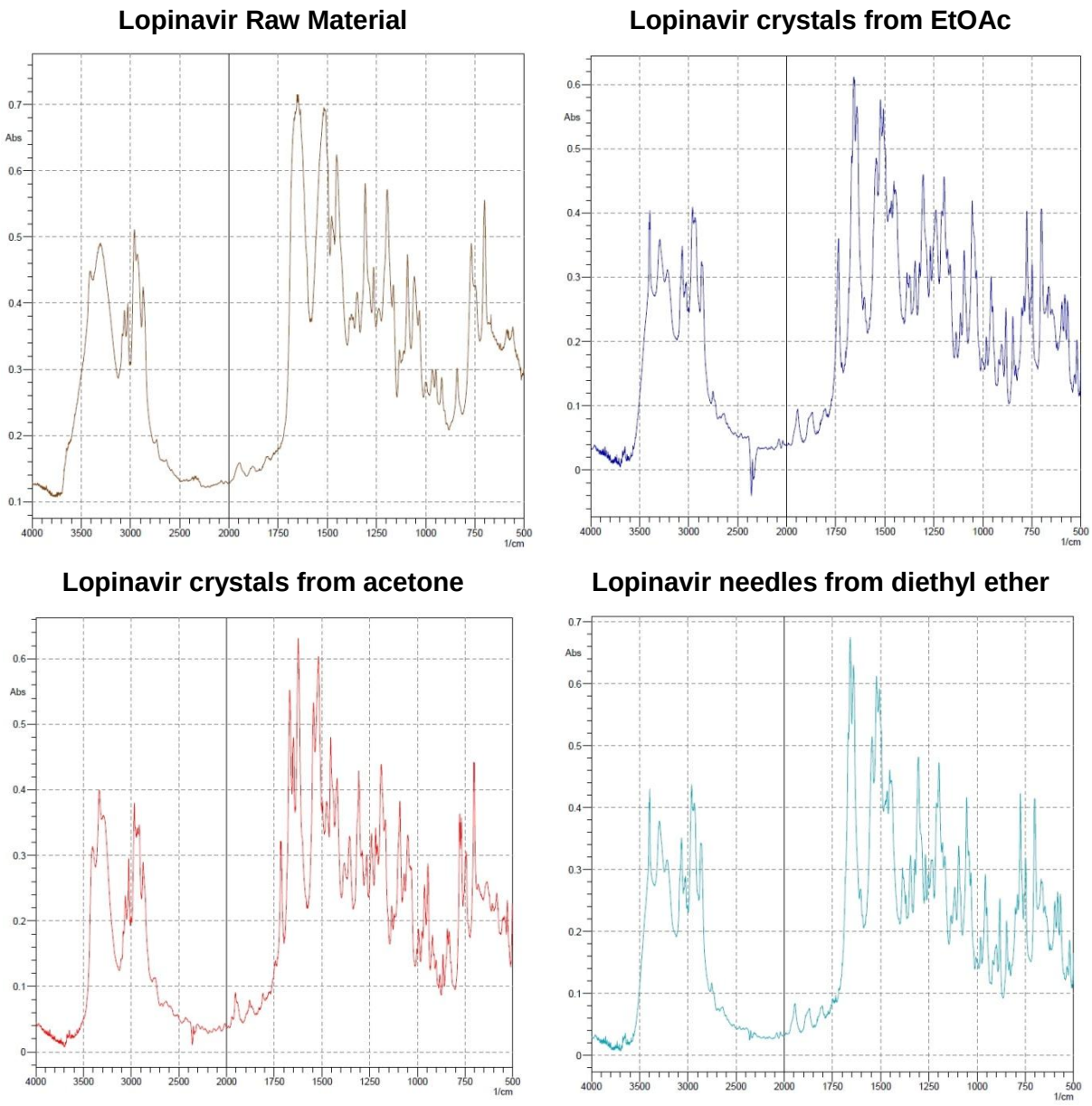

Figure 6.23: FTIR interferograms of lopinavir raw material and its recrystallisation products.

Unlike the interferograms obtained from didanosine and its recrystallisation products, the interferograms for lopinavir and its products differ quite significantly from each other. The known fact that the sharpness and intensity of the peaks are dependent on the crystallinity can clearly be seen when comparing these interferograms. Apart from the clear differences resulting from the amorphous and crystalline content of the samples, polymorphic differences are also evident from the interferograms. A peak appears between 1700 and 1750 cm^{-1} in the interferograms of only the predominantly crystalline samples, however, this peak shifts from 1717.68 cm^{-1} for the crystals obtained from acetone to 1737.94 cm^{-1} for those from ethyl acetate, possibly indicating an interaction on the carbonyl oxygen of either

the dimethylphenoxyacetyl or cyclic urea moiety (or possibly both). However, it is also possible that these peaks are the result of the entrapped solvent molecules' carbonyl oxygen groups. The origin of these peaks will be elucidated with SXRD analysis. Interestingly, this same peak is present in the interferogram of lopinavir glass cooled at ambient temperature (figure 6.24).

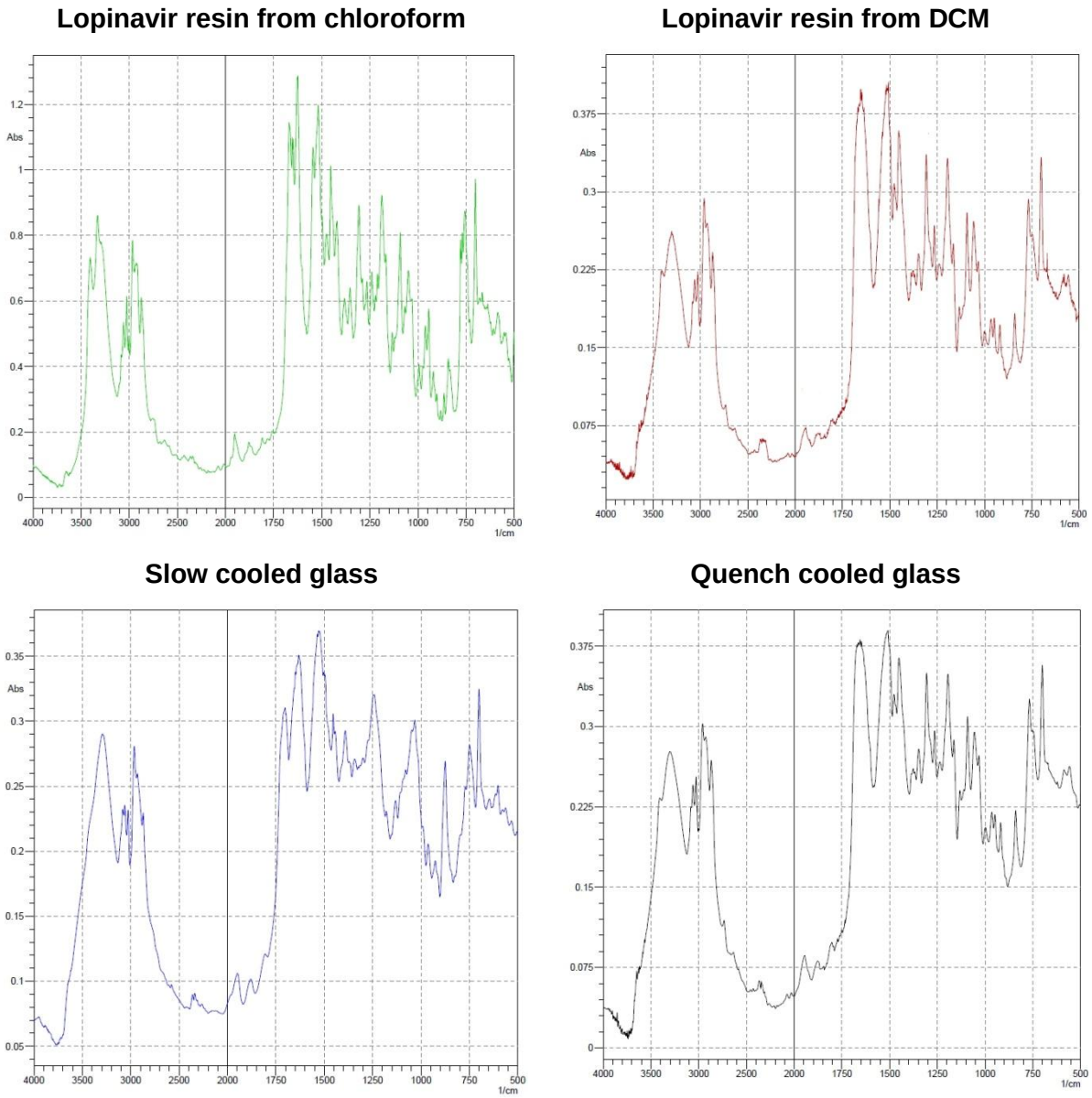

Figure 6.24: FTIR interferograms of lopinavir resins and glasses.

However, comparing the interferogram of the slow cooled glass to any of the other reported in this study clearly shows how disordered this glassy system is, with a heterogeneous dispersion of weak molecular interactions, as is evident from the broad, blunt peaks on its

interferogram relative to that of a more crystalline sample. The interferograms of the crystals from ethyl acetate and the needles from diethyl ether are strikingly similar, except for the peak at 1737.94 cm^{-1}, while the interferograms for the crystals from acetone and the resin from chloroform are similar, except for the peak at 1717.68 cm^{-1}. This indicates that these two sample "couples" share the same molecular interactions. An interesting find, since these "couples" have different unit cell dimensions on their PXRD diffractograms, indicating that the peaks found between 1700 and 1750 cm^{-1} play an important role in the polymorphism of lopinavir. The interferograms of the resin from dichloromethane and the quench cooled glass show that these preparations share the same molecular interactions as the raw material, an observation which is consistent with their PXRD diffractograms.

6.3.5 SXRD STUDY

SXRD data of the acetone crystals, as well as the ethyl acetate crystals, are presented here in table 6.4. The acetone crystal's unit cell contains four molecules of lopinavir and two molecules of acetone, accounting for the hemi-acetone solvate formulation given below in figure 6.25 B. All of the drug molecules in the crystal possess the same chirality, namely that with the *S*-configuration at each of the four chiral centres. Figure 6.25 A shows the structure and conformation of the lopinavir molecule in this solvate.

A **B**

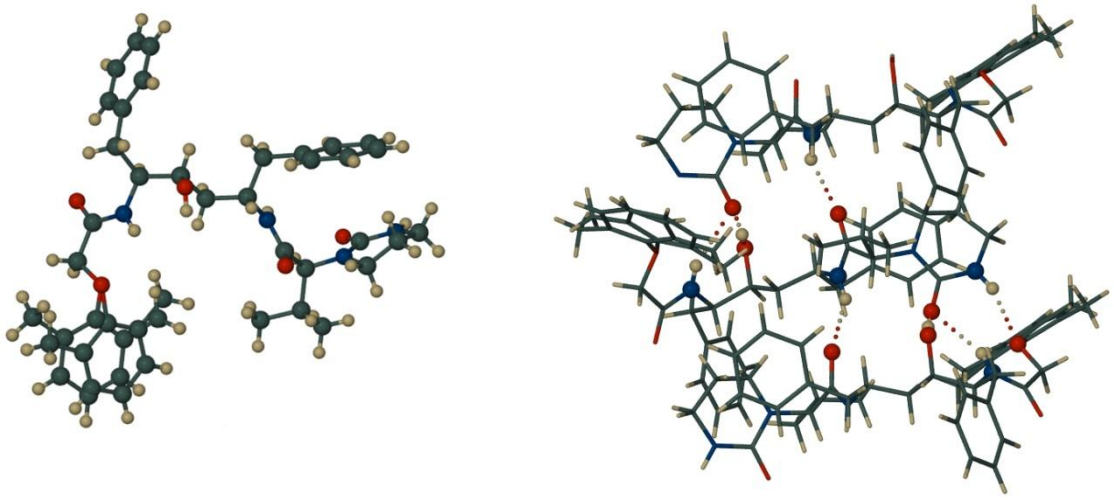

Figure 6.25: Structure and conformation of lopinavir in the acetone hemisolvate (A) and the intermolecular interactions holding the molecules together (B).

Modelling of the molecular structure was complicated by the twofold orientational disorder of the dimethyphenyl ring, with refined site-occupancies of the two components 54% and 46%.

There is extensive hydrogen bonding between the lopinavir molecules. Figure 6.25 B illustrates three molecules of the drug with several representative N-H···O and O-H···O hydrogen bonds linking them together. There are additional, weaker C-H···O hydrogen bonds (not shown) that contribute to the crystal stabilisation.

Table 6.4: Crystal data and structure determination statistics for lopinavir acetone hemisolvate

	Crystal Data	
Details	**Crystals from acetone**	**Crystals from EtOAc**
Formula	$2(C_{37}H_{48}N_4O_5)$, C_3H_6O	$2(C_{37}H_{48}N_4O_5)$, $C_4H_8O_2$
Formula Weight	1315.67	1345.69
Crystal System	Orthorhombic	Orthorhombic
Space Group	$P2_12_12$	$P2_12_12_1$
a, b, c (Å)	33.0091(16) 9.6895(5) 11.3774(6)	11.8979(4) 23.7016(7) 27.5845(8)
V (Å^3)	3639.0(3)	7778.8(4)
Z	2	4
Calculated crystal density (g/cm^3)	1.201	1.149
Mu (MoKa) (/mm)	0.080	0.078
F (000)	1416	2896
Crystal size (mm)	0.36 x 0.37 x 0.39	0.24 x 0.25 x 0.41
	Data collection	
Temperature (K)	173	173
Radiation (Å)	MoKa 0.71073	MoKa 0.71073
Theta Min-Max (°)	1.8, 28.3	1.7, 28.3
Dataset	-43: 34; -12: 10; -14: 15	-15: 11 ; -31: 27 ; -36: 31
Total, unique data, R (int)	21718, 5036, 0.032	35054, 19165, 0.032
Observed data [$I > 2.0\ \sigma\ (I)$]	4118	12870
	Refinement	
Nref, Npar	5036, 460	19165, 860
R, wR_2, S	0.0583, 0.1824, 1.10	0.0728, 0.2345, 1.00
Maximum and average shift/error	0.00, 0.00	0.00, 0.00
Flack x	0(10)	-0.2(10)
Min. and max. resd. dens. (e Å^{-3})	-0.44, 0.50	-0.31, 1.10

In figure 2.26, the included acetone molecules are highlighted in blue in space-filling mode while the drug molecules are shown in ball-and-stick mode. The solvent molecules are tightly

held within isolated sites along the crystallographic twofold axes (parallel to the *z*-direction), with their C=O groups lying on these axes.

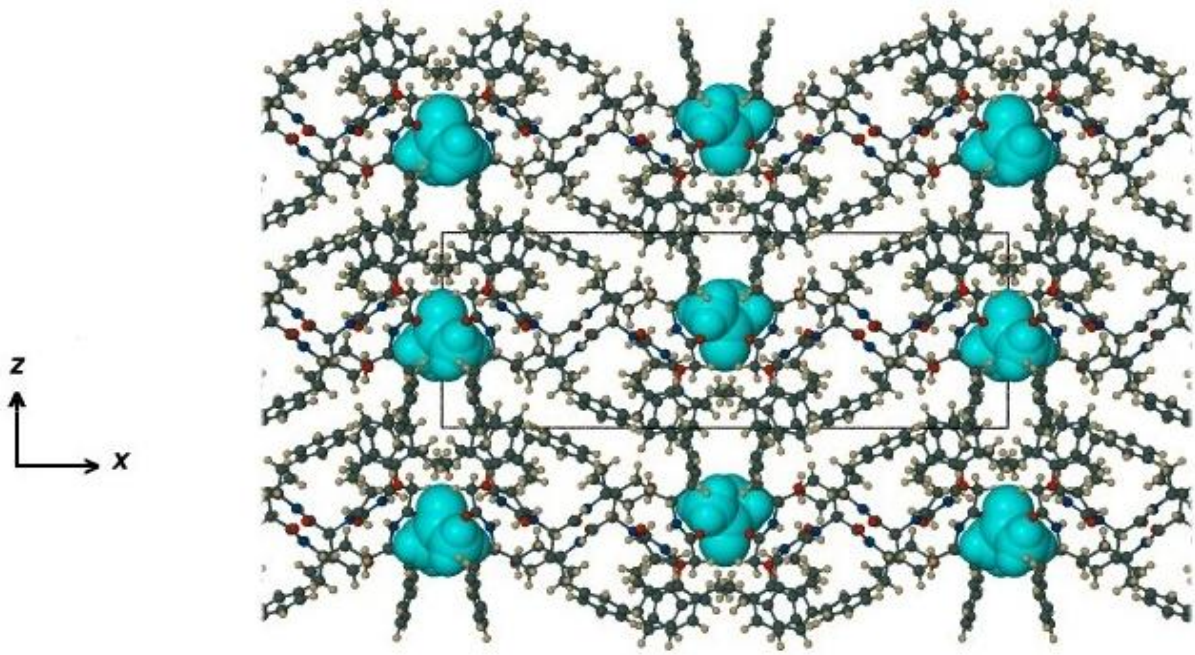

Figure 6.26: Three dimensional representation of lopinavir acetone hemisolvate's unit cells.

For the crystals obtained from ethyl acetate the crystal asymmetric unit (figure 6.27) comprises two independent lopinavir molecules as well as solvent. All of the chiral centres have the *S*-configuration. Figure 6.27 is not very informative due to extensive atomic overlap, but it is a record of the basic unit that is repeated by the operations of the space group. Crystallising in the orthorhombic space group $P2_12_12_1$, the unit cell of this phase thus contains 8 molecules of lopinavir and 4 molecules of ethyl acetate. Apart from the problems encountered with treatment of the solvent, there was relatively little molecular disorder. The latter consisted of a twofold disorder of a methylene group in the 2-oxo-1(*2H*)-pyrimidineacetamide residue of molecule A only (figure 6.27) corresponding to two alternative ring conformations. This was satisfactorily modelled (including the correct complement of H atoms in each case), the refinement giving a ratio of 57:43 for the two disordered components.

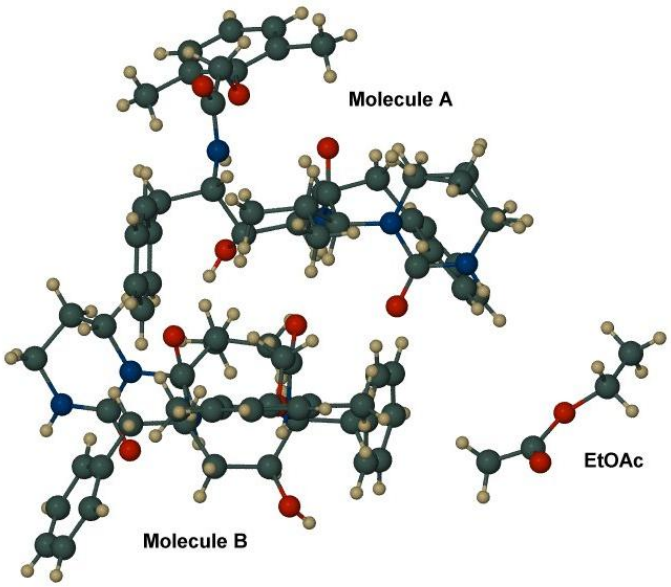

Figure 6.27: The crystal asymmetric unit of lopinavir crystals from ethyl acetate.

Hydrogen bonding in the crystal is very extensive and differs somewhat from that shown earlier for the acetone solvate. For example, one H-bond motif that occurs only in the ethyl acetate solvate is an amide-amide dimer, formed between two symmetry related A and B molecules (figure 6.28). For clarity all H atoms other than those involved in the motif described have been omitted. The full hydrogen bonding scheme could only be clearly illustrated in several figures featuring selected interactions. Also illustrated here is the minor disorder of a methylene group in the 2-oxo-tetrahydropyrimidinyl residue of molecule A.

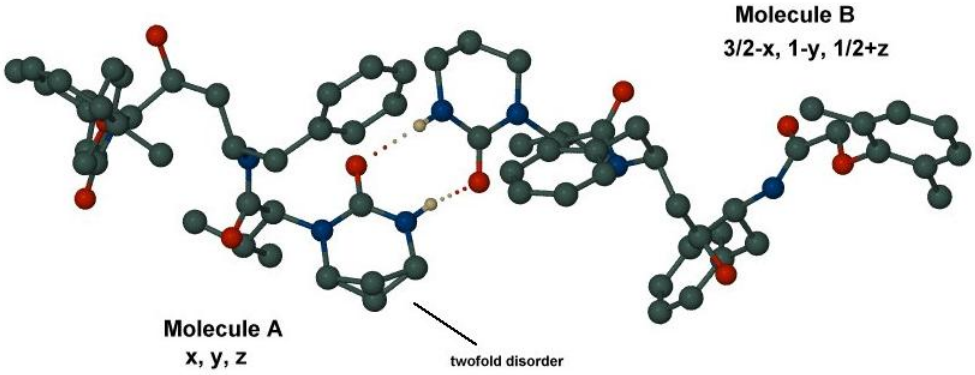

Figure 6.28: Amide-amide dimer in the lopinavir ethyl acetate solvate.

A packing diagram viewed down the a-axis is presented in figure 6.29. Lopinavir molecules are represented in ball-and-stick mode while the ethyl acetate molecules are drawn in space-filling mode. The solvent molecules are stacked in columns, each column being generated by the screw-axis parallel to the a-axis. The terminals of adjacent solvent molecules in the column are practically in contact with one another.

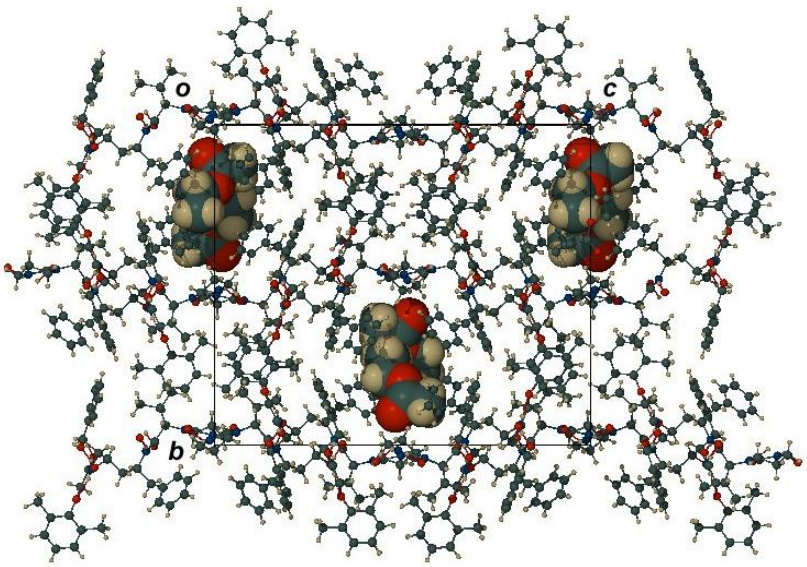

Figure 6.29: Packing diagram of the lopinavir ethyl acetate solvate.

The results of the SXRD analysis of the lopinavir solvates from acetone and ethyl acetate are consistent with their thermal analyses. The host (lopinavir) to guest molecule ratio is 2:1, which is consistent with the TGA of these crystals (although we reported a 2.57 ± 0.45 % weight loss for the crystals from ethyl acetate, subsequent TGA at UCT revealed a 6.7% weight loss, consistent with that of a hemisolvate). Furthermore, three dimensional modeling of the unit cells clearly show the acetone and ethyl acetate molecules to be caged in the crystal lattice, while forming no bonds with the lopinavir molecules. This explains the FTIR peak at 1717.68 cm^{-1}, the wavenumber associated with carbonyl oxygen absorption peaks. The other crystalline recrystallisation products (the needles from diethyl ether and the resin from chloroform) did not exhibit this peak, but the solvates from acetone and ethyl acetate did. The latter solvates' peaks between 1700 and 1750 cm^{-1} arise from the carbonyl oxygen of their guest molecules which does not undergo an interaction with the host molecules and is therefore free to absorb IR radiation at its natural frequency.

We wish thank Prof. Mino Caira of UCT for the exceptional SXRD work.

6.3.6 CONCLUSIONS FROM THE POLYMORPHISM STUDY

The thermal and x-ray data are quite conclusive in proving that all the recrystallisation products are polymorphs of each other, seeing as the raw material has no crystal structure. Based on the T_g's, the raw material, its glasses and recrystallisation products are all different amorphous forms of lopinavir raw material. The use of SXRD in elucidating the FTIR peaks found between 1700 and 1750 cm^{-1}, as well as corroboration of the thermal analysis show the importance of utilising a wide range of instruments to explore every possible outcome.

6.4 FRAGILITY STUDY

All the annealed DSC thermograms, from the raw material to the glasses prepared from the melt, presented a small enthalpy recovery endotherm preceding the glass transition. It was also mentioned in the thermal analysis section that these endotherms might be β-relaxations. This comes as little surprise, since we know from the work of Vyazovkin and Dranca (2006:425) that β-relaxations are not visible on a thermogram without annealing. Although this section will focus mostly on the fragility of the amorphous (and seemingly crystalline) lopinavir samples, β-relaxations and their significance to amorphous systems cannot be excluded from any study of amorphous material. Therefore, the first part of this section will deal exclusively with β-relaxations.

To investigate the β-relaxations, the method described by Vyazovkin and Dranca (2006:428), was used. After screening several heating rates, annealing temperatures and annealing times, the optimum conditions for investigating the β-relaxations of lopinavir were also found to be an annealing temperature of $0.8T_g$ and an annealing time of 20 minutes. Annealing of the samples above T_g caused a drastic decrease in the size of the β-relaxation endothermic peaks, making reliable and reproducible data gathering difficult.

Because of the inherently small endothermic peak of a β-relaxation, heating rates of 10-, 15- and 20 K/min were used to get the best resolution on the thermograms (figure 6.30). The samples were obtained from three independent batches, each analysed in triplicate. To minimise the effect of sample weight, all the samples in this study's weight were kept between 5 and 6 mg. The heating rate was limited to 20 K/min, since at this rate the β-relaxations of the lopinavir glass obtained from cooling at ambient temperature had already started to overlap with its glass transition (α-relaxation).

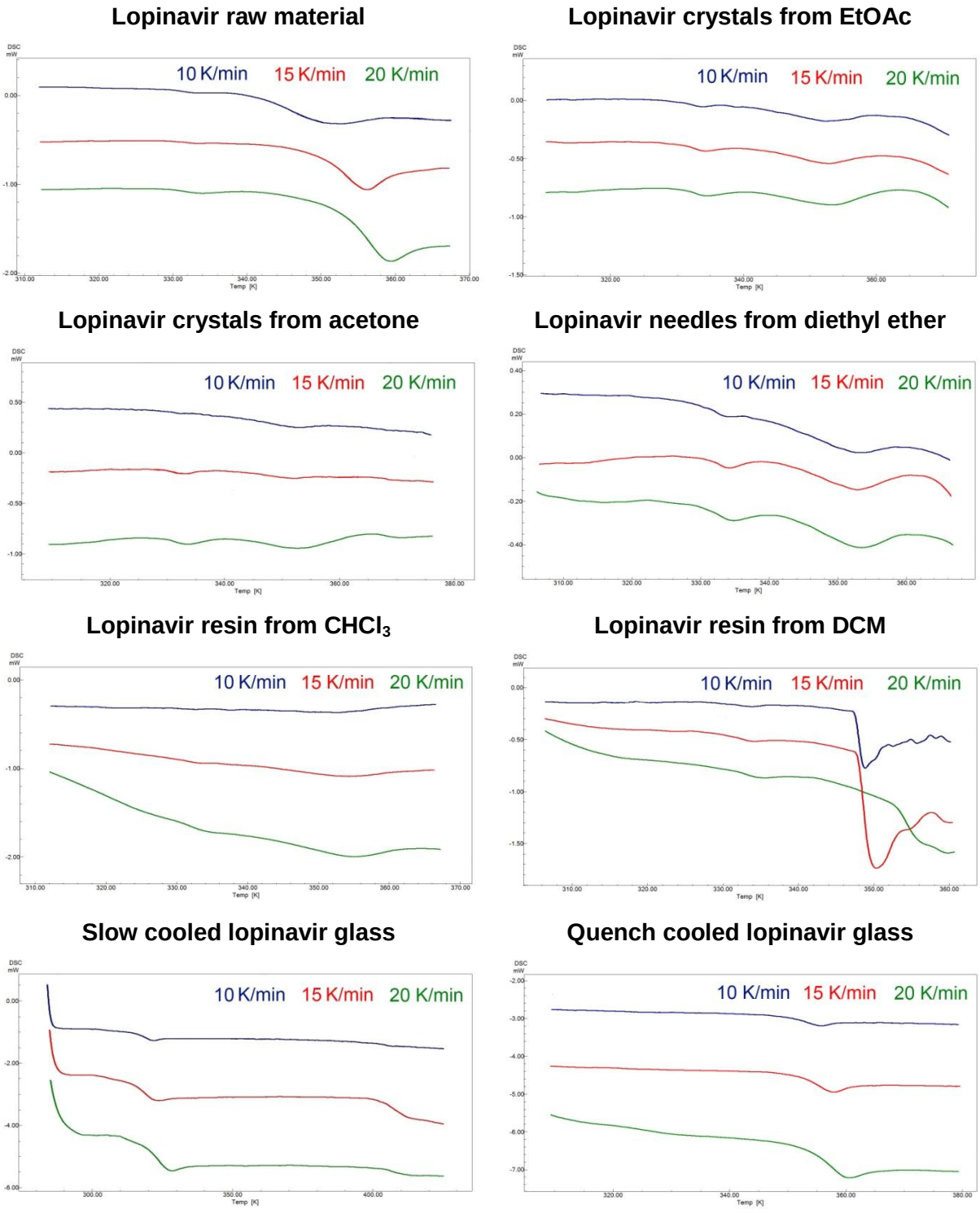

Figure 6.30: DSC thermograms of lopinavir raw material and its other preparations investigated in this study, showing the small β-relaxation endotherms in relation to the larger glass transitions.

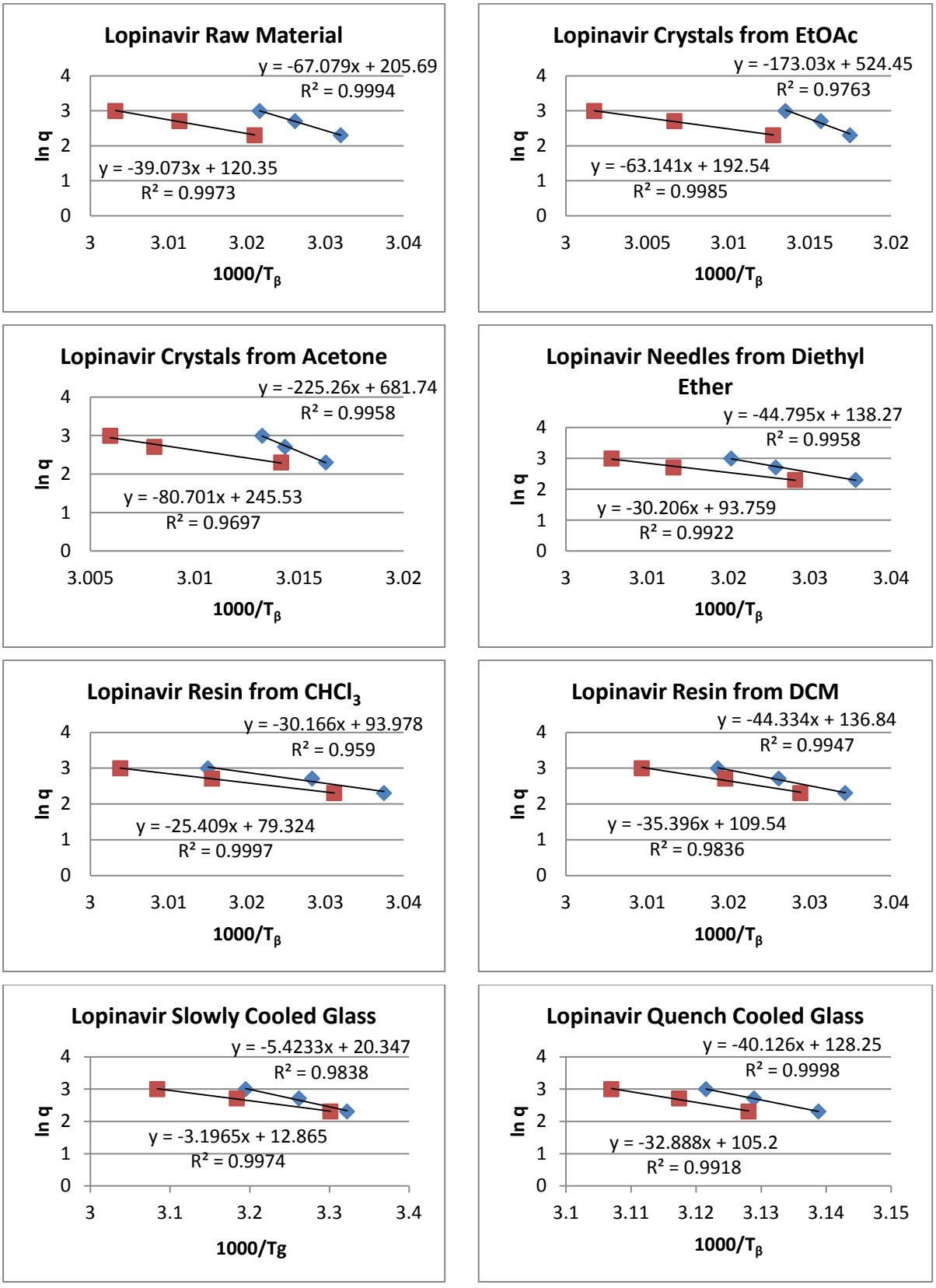

Figure 6.31: Arrhenius plots of T_β (blue rhombi) and T_β^{mid} (red squares) for each sample.

The β-relaxations were analysed exactly like glass transitions to obtain the β-relaxation temperature (T_β) and the temperature at the middle point of the β-relaxation process (T_β^{mid}). The importance of analysing both these temperatures, especially their relation to each other, will become clear shortly. The T_β of each sample at each heating rate is given in table 6.5. From these temperatures and heating rates the Arrhenius plots of each sample can be generated (figure 6.31). A lot of information can be gathered from the Arrhenius plots, especially when plotting both the onset temperature (T_β) and the temperature half way through the process (T_β^{mid}). Since the activation energy is directly proportional to the slope of the Arrhenius plot, it should be clear that slopes which progressively move away from each other are indicative of a stable material. The opposite is true for an unstable material, where the slope of the temperatures half way through the process approach the slope of the initial process temperatures. This can be seen when comparing the slopes of the lopinavir crystals to that of the lopinavir glass obtained from cooling at ambient temperature. However, this is just qualitative analysis and the purpose of the Arrhenius plots is to obtain the activation energy (table 6.5).

Apart from the activation energies for β-relaxation (ΔE_β) of the lopinavir crystals, the ΔE_β of the lopinavir raw material is the highest. Considering the fact that β-relaxations are the initial, local relaxations in a material which ultimately leads to a glass transition, the energy barrier imposed by ΔE_β is, in fact, the material's first line of defence against a glass transition. It should come as no surprise then that the raw material has a higher ΔE_β than the other amorphous samples prepared in this study, since the raw material is the form of lopinavir which remained stable during manufacturing, packing, shipping, handling and storage (for more than 3 years).

Concerning the crystals obtained from ethyl acetate and acetone, the ΔE_β actually gives a good representation of Ostwald's step rule. The crystals obtained from ethyl acetate grew much more rapidly than its acetone counterpart, therefore one would expect it to be the less stable of the two, and indeed less energy is required for the amorphous fractions in the crystals from ethyl acetate to undergo β-relaxations. The intra- and intermolecular interactions which stabilise the crystals from ethyl acetate over large ranges of order cannot protect it from short range molecular relaxations to the same extent as the more stable crystals from acetone can.

Next, let us investigate the global α-relaxations (glass transitions) and determine each material's fragility (m) and strength (D) parameters to see how it correlates to the local β-relaxations.

Table 6.5: T_β and T_β^{mid} of lopinavir raw material, its recrystallisation products and glass, as well as the activation energies of each

Preparation conditions	T_β (K)			T_β^{mid} (K)			ΔE_β (kJ/mol)	
	10 K/min	15 K/min	20 K/min	10 K/min	15 K/min	20 K/min	T_β	T_β^{mid}
Raw material	330 ± 1.56	330 ± 1.13	331 ± 0.01	331 ± 1.72	332 ± 0.78	333 ± 0.09	557	325
Ethyl acetate	331 ± 0.23	331 ± 0.47	332 ± 0.08	332 ± 0.19	333 ± 0.38	333 ± 0.22	1438	524
Acetone	331 ± 1.24	332 ± 0.02	332 ± 0.05	332 ± 0.89	332 ± 0.38	333 ± 0.04	1873	671
Diethyl ether	329 ± 0.17	330 ± 0.28	331 ± 0.22	330 ± 0.13	332 ± 0.29	333 ± 0.08	372	251
Chloroform	329 ± 1.64	330 ± 0.27	331 ± 0.27	330 ± 1.83	331 ± 0.24	332 ± 0.07	250	211
Dichloromethane	329 ± 1.72	330 ± 0.61	331 ± 0.52	330 ± 1.71	331 ± 0.59	332 ± 0.79	368	294
Slow cooled	301 ± 1.04	307 ± 1.49	313 ± 0.64	302 ± 3.14	314 ± 2.01	324 ± 0.08	45	26
Quench cooled	318 ± 0.66	319 ± 0.62	320 ± 0.39	320 ± 0.39	321 ± 0.08	322 ± 0.31	334	273

To investigate the fragilities of the different products obtained from lopinavir, as well as that of the raw material, the samples were annealed for 10 minutes at a temperature of 363 K. The samples were then cooled to 278 K and reheated at the same rate as which it was cooled, in accordance with the work by Moynihan *et al*. (1974:2673), Crichton and Moynihan (1988:413) and Crowley and Zografi (2001:83). The samples were run at heating rates of 5-, 10- and 20 K/min in triplicate and from three independent batches, the results of which are presented here in figure 6.32. To minimise the effect of sample weight on the position of the T_g, all the samples in this study's weight were kept between 5 and 6 mg.

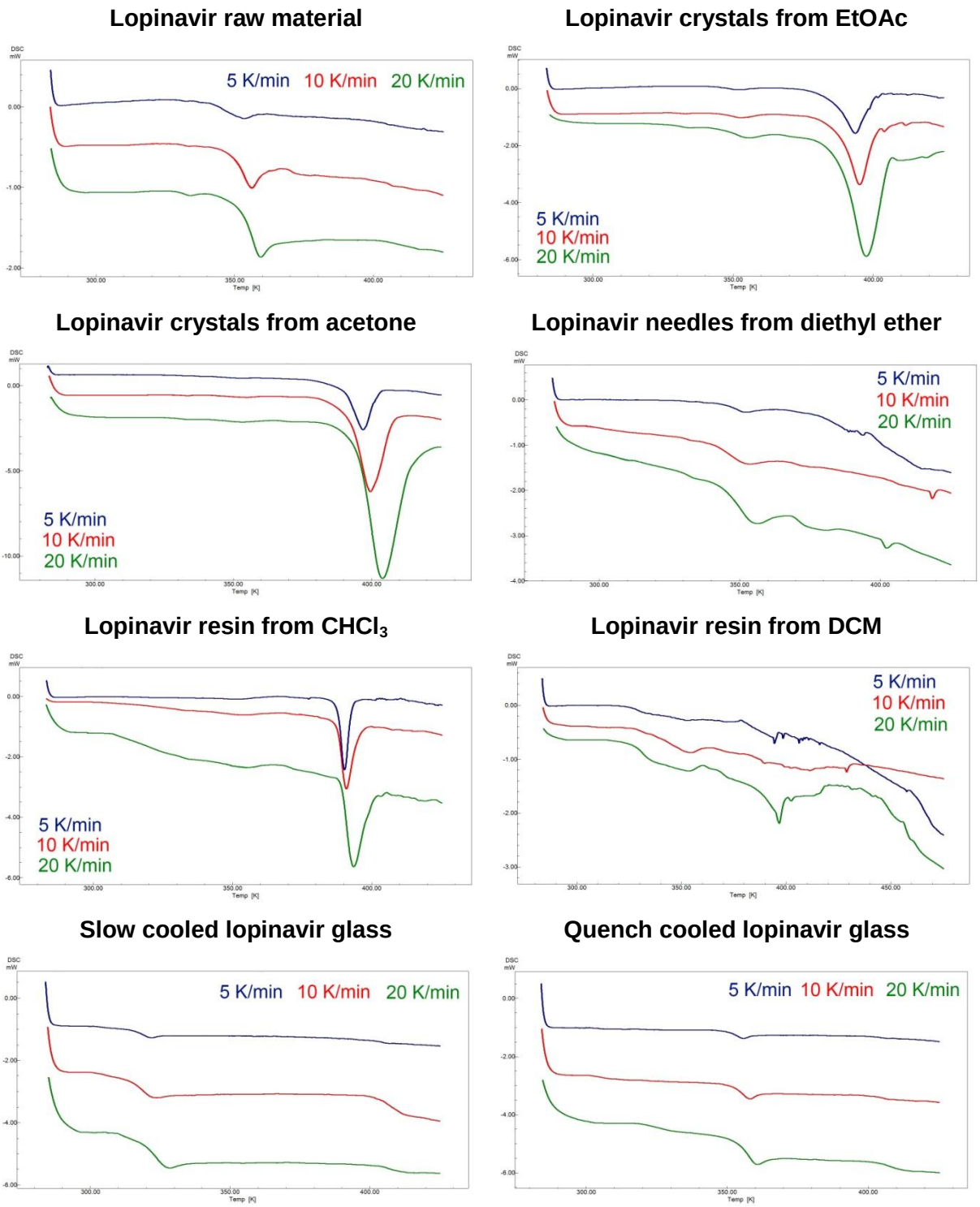

Figure 6.32: DSC thermograms of lopinavir raw material and its other preparations investigated in this study, showing the shifts in T_g with heating rate.

The average T_g and T_g^{mid} of each sample is given in table 6.6. The T_g of small molecule amorphous systems (which include many pharmaceuticals) can be used in much the same way as it is for polymers, that is, not only to identity the polymer but also to investigate the

stability of the system. In cases where the melting point of an amorphous solid is too close to its decomposition temperature or is undetectable, the melting temperature (T_m) can be substituted with the T_g to derive the same information. A higher T_g is indicative of a more stable material.

Table 6.6: T_g and T_g^{mid} of lopinavir raw material, its recrystallisation products and its glasses with relation to the different heating rates

Preparation conditions	T_g (K)			T_g^{mid} (K)		
	5 K/min	10 K/min	20 K/min	5 K/min	10 K/min	20 K/min
Raw material	344 ± 1.06	348 ± 0.41	353 ± 0.49	346 ± 1.01	351 ± 0.46	356 ± 0.28
Ethyl acetate	345.9 ± 0.36	346 ± 0.67	346.1 ± 0.61	347 ± 0.47	348 ± 0.15	349 ± 0.26
Acetone	349.6 ± 0.47	349.8 ± 0.06	349.9 ± 0.37	350.5 ± 0.7	350.8 ± 0.19	351.2 ± 0.19
Diethyl ether	336 ± 0.35	340 ± 2.36	342 ± 1.97	337 ± 0.39	343 ± 3.59	347 ± 3.19
Chloroform	336 ± 0.11	339 ± 2.82	342 ± 1.38	339 ± 0.64	344 ± 0.62	347 ± 0.09
Dichloromethane	327 ± 1.23	331 ± 6.61	336 ± 7.11	329 ± 0.78	336 ± 8.39	343 ± 4.72
Slow cooled	316 ± 0.58	318 ± 0.08	320 ± 0.19	319 ± 0.13	320 ± 1.64	322 ± 0.08
Quench cooled	350 ± 0.48	351 ± 0.39	353 ± 0.32	351 ± 0.38	354 ± 0.23	357 ± 0.15

From the shifts in T_g and T_g^{mid} relative to the heating rate, the Arrhenius plots of each sample were generated (figure 6.33).

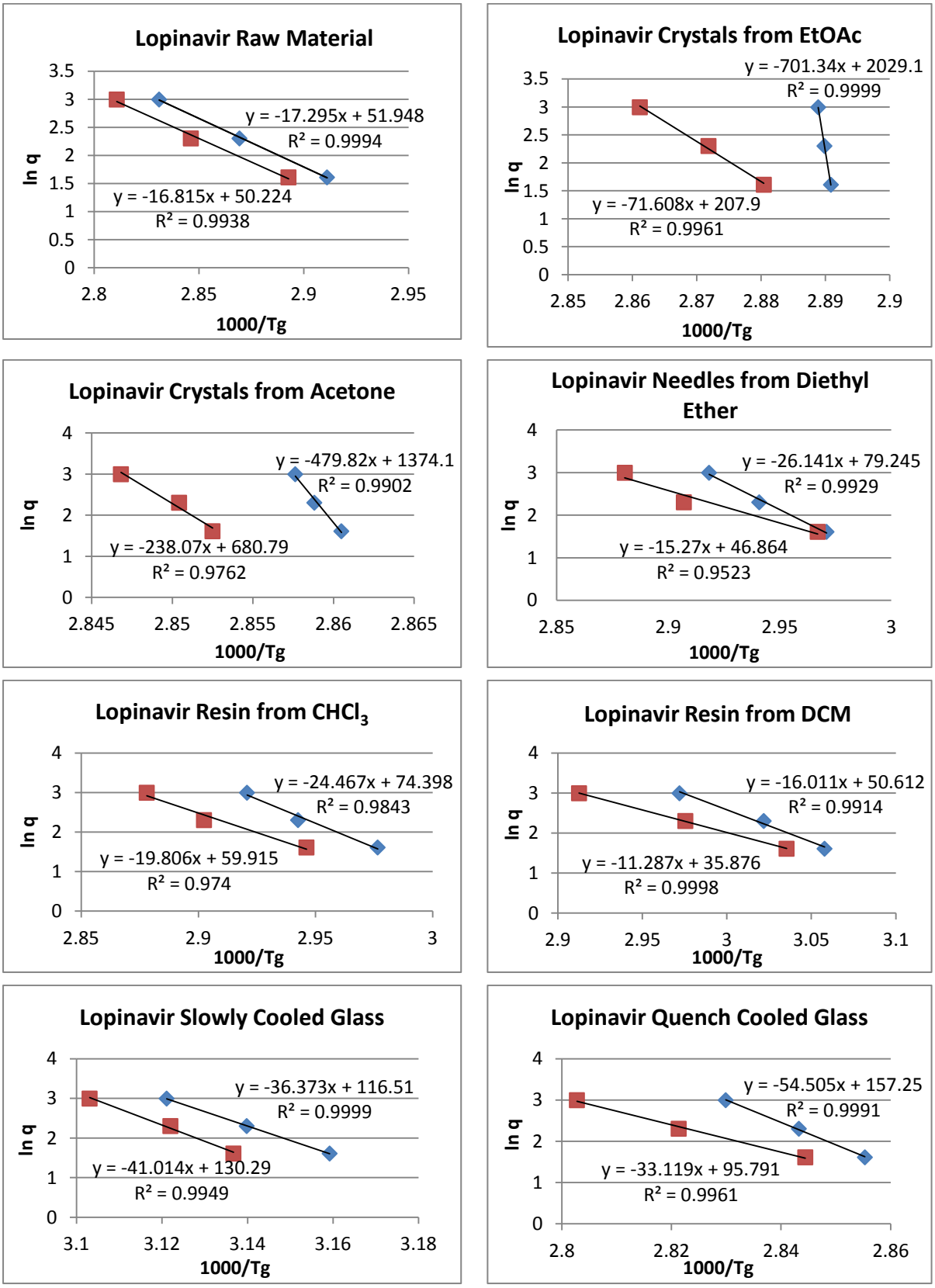

Figure 6.33: Arrhenius plots of T_g (blue rhombi) and T_g^{mid} (red squares) for each sample.

For the crystalline samples, one can clearly see the slopes progressively move away from each other, which is indicative of a stable material. The opposite can be seen for the lopinavir glass cooled at ambient temperature, where the slopes progressively move towards each other. The mere idea that the slopes might intersect is yet another indication of the instability of this glass. The question might arise then, why is this glass seemingly stable at room temperature over extended periods of time? The answer lies in the m and D values of the system. Turnbull and Fisher (1949:71) demonstrated that crystallisation from an amorphous material is primarily governed by the same factors that govern crystallisation from a melt. These factors can be illustrated by using the equation for heterogeneous nucleation (equation 6.1) from the melt. The rate of nucleation (I) is expressed as:

$$I = A\exp\text{-}(\Delta G_a + \Delta G^*)/kT \qquad (6.1)$$

Where ΔG_a is the activation energy for transport across the nucleus-amorphous matrix interface, ΔG^* is the free energy change for nucleation with a critical nucleus of radius r, A is a constant, k is the Boltzmann constant and T is the temperature. The numerator in the exponent of equation 6.1 has the same function as activation energy (ΔE_a) in the Arrhenius equation (6.2), and it has already been illustrated in equations 4.4 and 4.5 that m is directly proportional to ΔE_a and D is inversely related to m.

$$k = A\exp\text{-}\Delta E_a/RT \qquad (6.2)$$

The glass cooled at ambient temperature displays a higher m and lower D value (table 6.7) than those of the other amorphous samples prepared in this study, making it the second most stable amorphous form in this study, second only to the quench cooled glass. However, the m and D values are only indicative of the stability of a system at temperatures near its T_g, and does not take into account the lower energy β-relaxations which lead to the glass transition. To obtain the full picture, local and global relaxations need to be correlated with each other. Case in point, if only the ΔE_a for T_g was used to determine the stability of the glass cooled at ambient temperature, the system would seem stable over extended periods of time which, in storage (with minimum energy fluctuations and agitation) it is, but the influence of short term energy fluctuations and its immediate impact on the system would be ignored. These effects can be readily deduced from ΔE_β and could potentially play an important role in understanding short time scale changes in the system, for example during milling and dissolution. The necessity of determining both (ΔE_β) and the ΔE_a for T_g will become clear during the solubility study. The m and D parameters of each sample are presented here in table 6.7.

Table 6.7: Activation energies lopinavir raw material, its recrystallisation products and its glasses, as well as the fragility (m) and strength (D) parameters of each

Preparation conditions	ΔE_a (kJ/mol)		m	D
	T_g	T_g^{mid}		
Raw material	144	140	21	106
Ethyl acetate	5831	595	880	1
Acetone	3989	1979	561	1
Diethyl ether	217	126	33	34
Chloroform	203	165	31	39
Dichloromethane	133	94	20	130
Slow cooled	302	340	50	17
Quench cooled	453	275	67	11

The ΔE_a for T_g and T_g^{mid} of the crystalline samples are exceptionally high. However, one must remember that the activation energy is determined from the slope of the Arrhenius plot and the slope is dependent on the rate of change (in this case, the rapidness of T_g and T_g^{mid}) in the investigated parameter. Both these samples are crystalline and contain only a small amount of amorphous material. Because the amorphous fraction is so small, the rate at which it relaxes is much more rapid than that of samples containing predominantly amorphous material. With that being said, high ΔE_a for global molecular motions in these two samples are not entirely unexpected since both are crystalline, and contain large volumes with long range order which could extend into the smaller amorphous regions and stabilise it. The lopinavir resin obtained from dichloromethane was the strongest glass (highest D value), indicating that it was more pliable and less likely to break, while also displaying significant resistance to local molecular motion (ΔE_β of 368 kJ/mol). This was also the sample which retained its gum-like properties the longest without signs of crystallisation, showing good coherence between the thermal and macroscopic observations. Of all the amorphous samples, the quench cooled lopinavir glass exhibited the highest fragility, and was also the sample which presented itself macro- and microscopically as broken glass. The raw material had the second lowest m and second highest D values of all the samples

analysed, because of its low ΔE_a for T_g and T_g^{mid}, making it the second most unstable. This instability can explain the ability of the lopinavir raw material to yield the amount of different amorphous and crystalline forms obtained in this study, since recrystallisation involved high temperatures, significantly increasing the global molecular mobility of the lopinavir molecules in the solute particles. If not for the β-relaxation study, one might assume that the raw material was simply the second most unstable, while it is actually the amorphous system with the highest resistance to local molecular motion (ΔE_β of 557 kJ/mol), explaining how it could withstand the energy fluctuations of manufacturing, shipping and handling. Micrographs of the resin obtained from chloroform (figure 6.12) showed large amounts of small crystallites scattered throughout the amorphous matrix. Although ΔE_a for T_g and T_g^{mid} values suggest that this sample is moderately stable, it exhibited an ΔE_β of 250 kJ/mol, which was significantly less than that of the resin obtained from dichloromethane, and the second lowest ΔE_β overall. This explains the presence of crystallites in the resin from chloroform, and why they are not present in the resin obtained from dichloromethane. Increased molecular motilities in local regions within the amorphous matrix facilitated nucleation, and lead to the growth of crystallites.

6.5 CALCULATION OF AMORPHOUS CONTENT

To calculate the amorphous content of each sample, the method reported by Lefort *et al*. (2004:211) was employed. This is the logical starting point, since the method is based on first principles, and does not require a calibration trace. The samples were analysed in triplicate and from three individual batches at heating rates of 10 K/min. The data obtained from the thermal analyses, as well as the calculated amorphous fractions (τ_{DSC}) are given in table 6.8.

The method described by Lefort *et al*. (2004:211) to calculate the amorphous fraction of a solid requires the DSC thermogram of the solid in question to exhibit a recrystallisation exotherm and a melting endotherm, as well as the constraint that this crystallisation and melting do not spread over a large temperature range. For this reason, the τ_{DSC} of lopinavir raw material (figure 6.2) and its glasses (figures 6.16 and 6.18) could not be determined using this method. Fortunately, the thermograms of the lopinavir recrystallisation products do adhere to these constraints and their τ_{DSC} could be calculated, bearing in mind that in the absence of a fully crystalline sample, the lopinavir crystals obtained from acetone were used as the most crystalline reference.

Table 6.8: Calculation of the amorphous fraction of lopinavir recrystallisation products

Preparation medium	$\Delta H_{cr}(T_{cr})$	$\Delta H_m(T_m)$	Weight (mg)	τ_{DSC}
Acetone	0.3 ± 0.03	42.3 ± 1	4.5 ± 0.17	1
Ethyl acetate	0.6 ± 0.04	27.9 ± 1.14	5.4 ± 0.96	2.7
Chloroform	0.8 ± 0.04	7.7 ± 1.53	5.6 ± 0.69	14.4
Diethyl ether	0.4 ± 0.74	0.6 ± 0.02	5.2 ± 0.82	78.8
Dichloromethane	0.4 ± 0.9	0.5 ± 0.04	4.9 ± 0.68	127.2

These crystals have already been proven to be the most crystalline, both in the preceding sections of this chapter and here, as can be seen by its $\Delta H_{cr}(T_{cr})$ and $\Delta H_m(T_m)$ values. We know from the thermal analysis that these crystals are not only partially amorphous, but also hemisolvates. Therefore, their melting endotherm is partially the result of desolvation, meaning that the true melting endotherm (that of a dry sample) would have a smaller value than its current $\Delta H_m(T_m)$. However, it has been proven by thermal analysis and SXRD studies that the solvent is entrapped so tightly in the crystal structure that it is only released upon melting, making it impossible to obtain a dry sample for analysis. Coupled with the fact that a fully crystalline sample would, in any case, present a larger melting endotherm than a desolvated crystal, and that the aim of this part of the study is only to obtain reliable, comparative data for use later on in this chapter, the crystals from acetone were used as reference for the most crystalline sample.

Because of polymorphic differences in the unit cell dimensions of all the lopinavir samples displaying peaks on PXRD, the methods described in section 4.7 to calculate the crystalline and amorphous content were not used in this study. The methods described by Black and Lovering (1977:684) and Saleki-Gerhardt *et al*. (1994:237) was developed around a fully crystalline sample, a fully amorphous sample and known mixtures of the two. In other words, the polymorphism of the crystalline content was constant. The methods entail identification of peaks which change in intensity with amorphous content and peaks whose intensities remain constant regardless of crystalline or amorphous content. The methods do not account for shifts in peak positions because of polymorphic differences and, since shifts in peak positions could cast doubt on the comparability of these peaks' intensities, these methods were omitted.

It was decided to still use the FTIR method described by Black and Lovering (1977:684) because, even though this method also relies on identification of peaks which are dependent on crystallinity and peaks which are independent on crystallinity, a full spectrum FTIR scan at high Fourier numbers will give a detailed description of the molecular interactions in the sample. These FTIR scans give more data points to work with and peak shifts resulting from polymorphism can be reliably filtered. For example, obvious peaks found between 1700 and 1750 cm^{-1} for the crystals from ethyl acetate and acetone, which might at first glance seem the obvious choice but, have already been proven to arise from the unbound carbonyl oxygen of the solvents entrapped in the crystal lattice.

After filtering peaks based on polymorphic shifts in positions, only a few peak options remained for investigation of amorphous/crystalline content. The peak at 701.15 cm^{-1} remained constant in position and intensity and was used as the independent peak. However, this peak is very close to the finger print region of the interferogram and other alternatives were investigated. The band at 2964 cm^{-1} was also identified as being independent on crystallinity and did not shift in position. The peak at 1650 cm^{-1} was only barely visible on the interferogram of the quench cooled glass, increased slightly on the interferograms of the other predominantly amorphous samples and was clearly visible for the more crystalline samples. This peak was therefore taken as the peak which was dependent on crystallinity. The samples were analysed according to the method described by Black and Lovering (1977:684) and the data is presented here in table 6.9.

Table 6.9: The corrected peak intensities and ratios of the FTIR interferograms

Preparation medium	Corrected relative intensities			Ratio	
	1650	701	2964	1650:701	1650:2964
Acetone	0.26 ± 0.072	0.21 ± 0.056	0.16 ± 0.023	1.29 ± 0.142	1.68 ± 0.118
Ethyl acetate	0.23 ± 0.021	0.18 ± 0.016	0.15 ± 0.02	1.26 ± 0.135	1.57 ± 0.131
Chloroform	0.39 ± 0.051	0.37 ± 0.045	0.27 ± 0.047	1.05 ± 0.051	1.44 ± 0.075
Diethyl ether	0.15 ± 0.008	0.22 ± 0.014	0.19 ± 0.009	0.77 ± 0.044	0.87 ± 0.059
Dichloromethane	0.02 ± 0.003	0.11 ± 0.015	0.09 ± 0.01	0.24 ± 0.038	0.25 ± 0.035

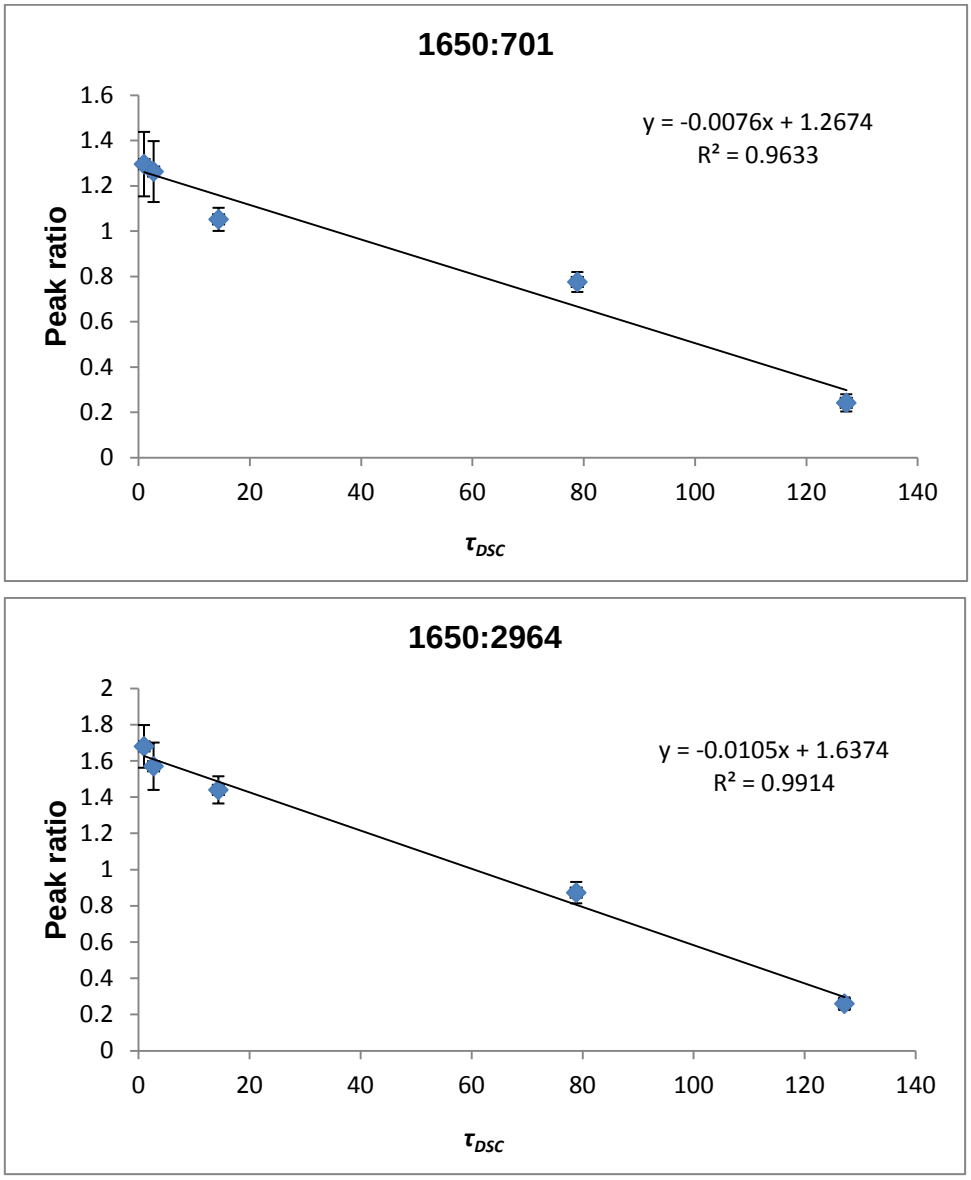

Figure 6.34: Linear regression of the peak intensity ratios and the τ_{DSC}.

The ratios of the peak intensities can be used for multiple purposes, such as the determination of the τ_{DSC} for lopinavir raw material and its glasses which did not exhibit a melting endothermic peak on their DSC thermograms. For a long time now, it has been known that there exists a linear relationship between the peak intensities (on both PXRD diffractograms and FTIR interferograms) and the amount of amorphous/crystalline content in the sample. By plotting the ratios of the peak intensities from table 6.9, to the τ_{DSC} calculated in table 6.8, one would expect a linear decrease in the peak intensity ratio corresponding to an increase in τ_{DSC}. The results of the linear regressions are given in figure 6.34. The linear regression can also serve the purpose of verifying the τ_{DSC} values, since a good fit between results depicting the same answers (in this case amorphous content) but obtained from

instruments operating on different principles, not only indicates that the results are comparable, but also reliable. From the straight line equation of the trend line, the τ_{DSC} of lopinavir raw material and its glasses can be calculated. From the peak ratios of lopinavir raw material, slow cooled glass and quench cooled glass (0.29 ± 0.06, 0.1 ± 0.015 and 0.07 ± 0.001 respectively), τ_{DSC} values of 128.25, 146.35 and 148.49 respectively are calculated. Although the τ_{DSC} values of lopinavir's glasses are quite low, they are still some values off from the x-intercept of 155.94.

To investigate the possibility of these glasses containing some crystalline material, light microscopy was employed (figure 6.35).

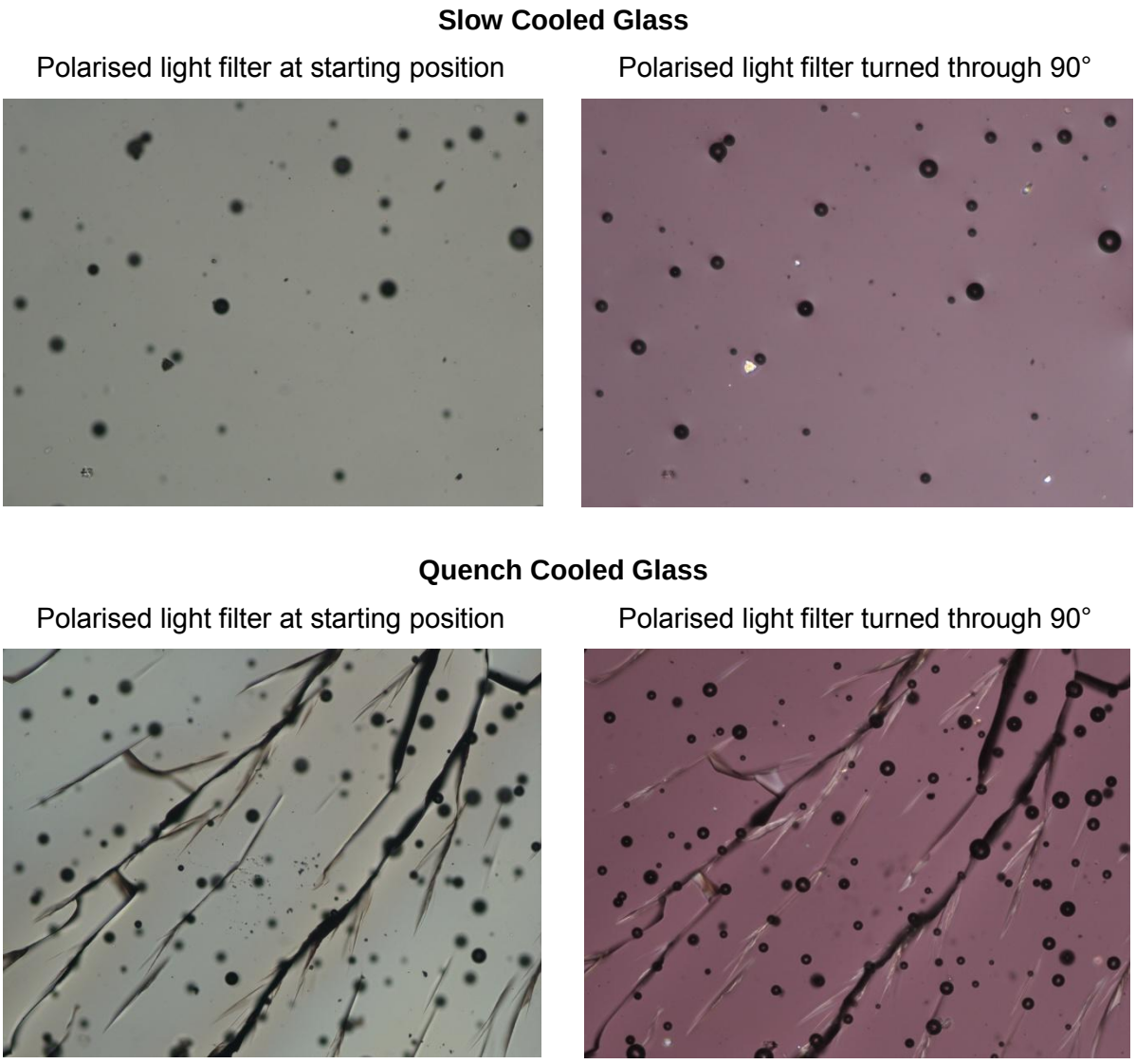

Figure 6.35: Micrographs of lopinavir glasses showing crystalline content.

The influence of dislocations on the surface of the glass, created in this manner, on the solubility would be interesting to investigate. With a thorough investigation of the physicochemical properties of lopinavir raw material, its glasses and recrystallisation products completed, it was decided to investigate the solubility of each sample and see if the amorphous content has an effect on the solubility.

6.6 SOLUBILITY STUDY

The peptidomimetic structure of lopinavir also has an influence on the bioavailability of the drug. Lopinavir is weakly soluble in water, has low permeability, is extensively metabolised in the liver and is 98 – 99 % bound to plasma proteins. Ritonavir is added to the commercial preparation to inhibit the hepatic metabolism of lopinavir and solid-state properties cannot influence the plasma protein binding of the drug. However, manipulation of the solid-state properties can possibly increase the aqueous solubility of the drug. In this section, we will investigate the solubility of each lopinavir sample in double distilled water, 0.1 N HCl and ethanol.

To investigate the solubility of lopinavir raw material, its glasses and recrystallisation products, six oversaturated solutions of each were prepared and stirred for 24 hours at 310 K in a water bath. The time span of 24 hours was chosen as this represented the maximum amount of time needed for the sample to reach equilibrium solubility. The oversaturated solutions were prepared from double distilled water, 0.1 N HCl and ethanol. The standard curves for lopinavir in the different solution media are presented here in figure 6.36.

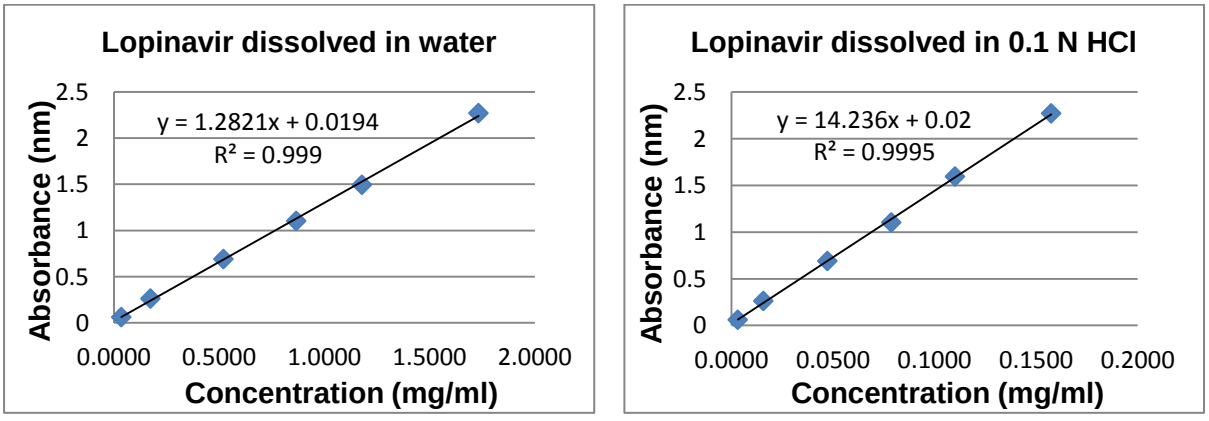

Figure 6.36: Standard curves for lopinavir.

Lopinavir raw material, its recrystallisation products and glasses were extremely soluble in ethanol, all in excess of 2 grams per ml at room temperature. This made preparation of sufficient amounts of sample to test for ethanol solubility impractical. The results from the solubility study are given in table 6.10.

Table 6.10: Solubility of lopinavir raw material, glasses and recrystallisation products

Sample preparation conditions	Solubility (mg/ml)	
	Water	**0.1 N HCl**
Raw Material	0.054 ± 0.0072	0.066 ± 0.005
Ethyl acetate	0.02 ± 0.0066	0.02 ± 0.0044
Acetone	0.024 ± 0.0062	0.024 ± 0.0019
Diethyl ether	0.055 ± 0.0036	0.066 ± 0.0089
Chloroform	0.058 ± 0.0088	0.064 ± 0.0099
Dichloromethane	0.026 ± 0.0016	0.028 ± 0.0072
Slow Cooled Glass	0.093 ± 0.009	0.104 ± 0.0045
Quench Cooled Glass	0.035 ± 0.006	0.042 ± 0.0061

The lopinavir glass obtained from cooling of the melt at ambient temperature displayed a 72 % increase in solubility, followed by the resin obtained from chloroform, which exhibited only a 7 % increase in solubility relative to the raw material. A histogram of the data reported in table 6.10 is given in figure 6.37. Interestingly, there is no direct correlation between the aqueous solubility of lopinavir and its amorphous content. This seems to be at odds with the general notion that solubility increases with an increase in amorphous content.

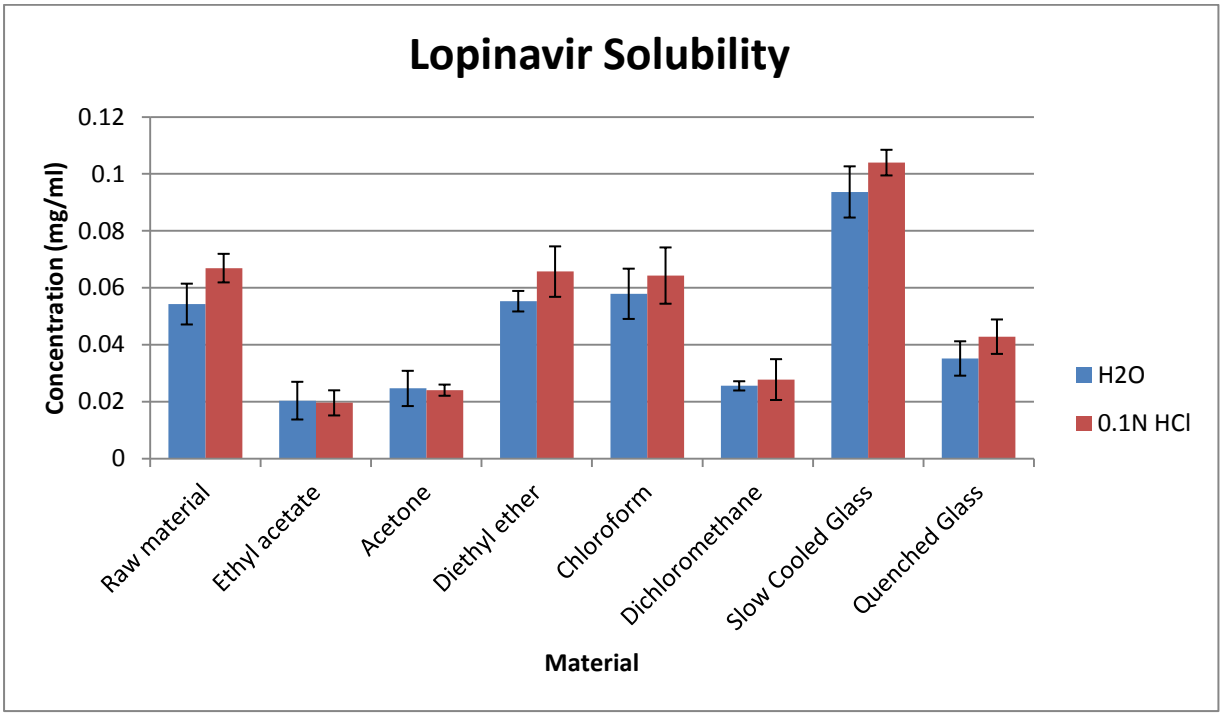

Figure 6.37: The solubility of lopinavir raw material, glasses and recrystallisation products.

Although the amorphous samples did display better aqueous solubility than the crystalline samples, several inconsistencies appear when looking more closely at the amorphous content. The quench cooled glass, which has been proven to be the most amorphous of all the samples, did not display the best solubility, while the resin from chloroform, which has been proven to contain relatively small amounts of amorphous material, exhibited the second highest aqueous solubility. Clearly the aqueous solubility is governed by some other factor(s).

There is also no correlation between the fragility and solubility of the samples, which is not too surprising considering the fact that the fragility data was obtained from the T_g's of the samples, at temperatures much higher that the conditions under which the solubility study were performed. However, there is a correlation, albeit an inverse one, between the solubility and ΔE_β of each sample (figure 6.38). This observation makes perfect sense, considering that the ΔE_β is, in essence, only an energy barrier preventing local molecular motions from occurring. If this energy barrier is breached, the solvent can take advantage of the local increased molecular motions on the surface of the sample, since an increase in molecular motion would decrease the contact angle, and facilitate its dissolution. Removal of molecules from the surface of the sample can cause the formation of dislocations, leading to surface roughening and increasing the effective surface area, thereby increasing its solubility.

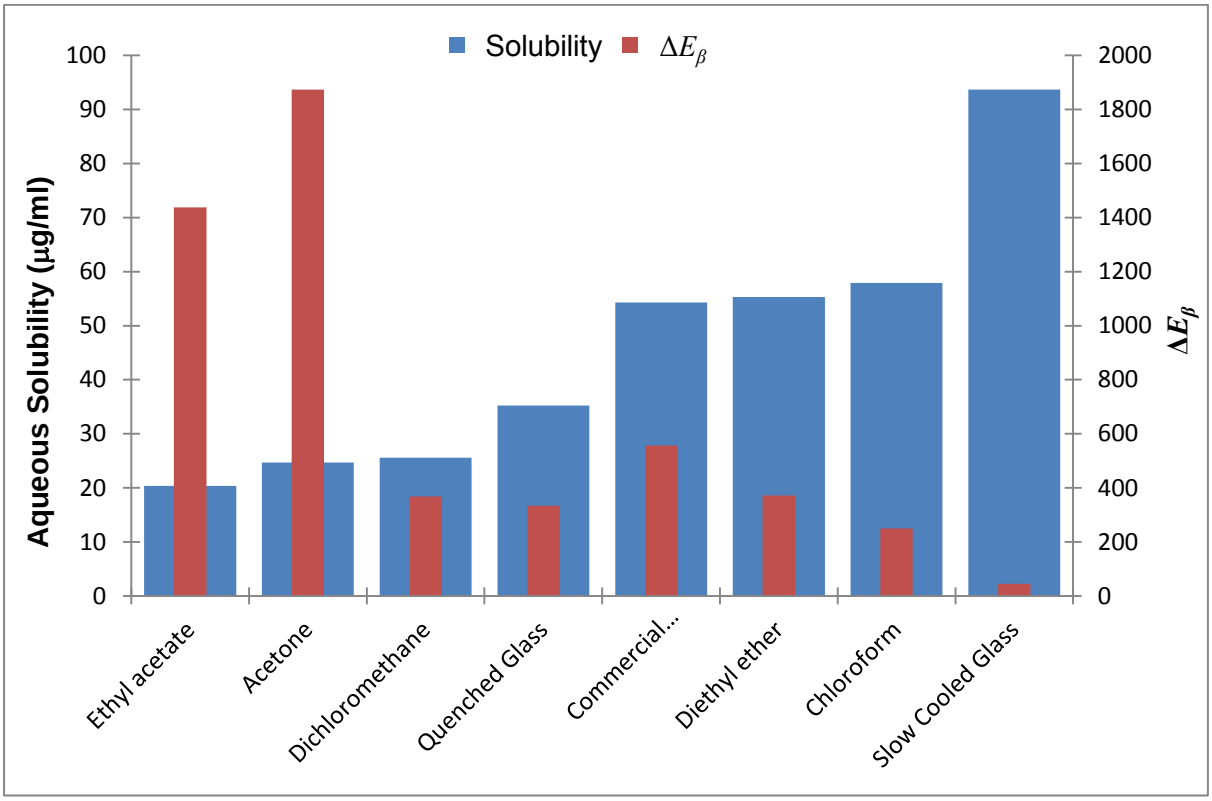

Figure 6.38: Histogram depicting the inverse correlation between solubility and ΔE_β.

6.7 CONCLUDING REMARKS

This study presents the first detail physicochemical analysis and polymorphism screening of lopinavir. Four new polymorphs were obtained and three unique amorphous forms were prepared. This study also illustrates the necessity of conducting a thorough investigation into every possible parameter that could influence a physical or chemical property. If only the amorphous content and/or global molecular relaxations (glass transitions) were investigated, no explanation for the solubility behaviour of lopinavir would have been found. The use of multiple instruments, operating on different principles, to obtain comparable results and thereby increase the reliability of the results is also illustrated. Apart from a detailed physicochemical analysis, a previously unknown correlation between ΔE_β and solubility is presented in this study. The knowledge obtained concerning the influence of ΔE_β on the solubility of amorphous lopinavir can be of significant importance to future work on other amorphous pharmaceuticals.

REFERENCES

BLACK, D.B. & LOVERING, E.G. 1977. Estimation of the degree of crystallinity in digoxin by X-ray and infrared methods. *Journal of pharmacy and pharmacology*, 29:684-687, Apr.

CRICHTON, S.N. & MOYNIHAN, C.T. 1988. Dependence of the glass transition temperature on heating and cooling rate. *Journal of non-crystalline solids*, 99(2-3):413-417, Feb.

CROWLEY, K.J. & ZOGRAFI, G. 2001. The use of thermal methods for predicting glass-former fragility. *Thermochimica acta*, 380:79-93.

DICKMAN, D.A., CHEMBURKAR, S., FORT, J.J., HANRY, R.F., LECHUGA-BALLESTEROS, D., NIU, Y. & PORTER. W. 2007. Crystalline pharmaceutical. Patent: US 2007/0027172 A1. 49 p.

KEMPF, D.J., MARSH, K.C., DENISSEN, J.F., MCDONALD, E., VASAVANONDA, S., FLENTGE, C.A., GREEN, B.E., FINO, L., PARK, C.H., KONG, X.-P., WIDEBURG, N.E., SALDIVAR, A., RUIZ, L., KATI, W.M., SHAM, H.L., ROBINS, T., STEWART, K.D., HSU, A., PLATTNER, J.J., LEONARD, J.M. & NORBECK, D.W. 1995. ABT-538 is a potent inhibitor of human immunodeficiency virus protease and has high oral bioavailability in humans. *Proceedings of the Natural Academy of Sciences of the United States of America,* 92(7):2484-2488, Mar.

KEMPF, D.J., MARSH, K.C., KUMAR, G., RODRIGUES, A.D., DENISSEN, J.F., MCDONALD, E., KUKULKA, M.J., HSU, A., GRANNEMAN, G.R., BAROLDI, P.A., SUN, E., PIZZUTI, D., PLATTNER, J.J., NORBECK, D.W. & LEONARD, J.M. 1997. Pharmacokinetic enhancement of inhibitors of human immunodeficiency virus protease by coadministration with ritonavir. *Antimicrobial agents and chemotherapy*, 41(3):654-660, Mar.

MOLLA, A., KORNEYEVA, M., GAO, Q., VASAVANONDA, S., SCHIPPER, P.J., MO, H.-M., MARKOWITZ, M., CHERNYAVSKIY, T., NIU, P., LYONS, N., HSU, A., GRANNEMAN, G.R., HO, D.D., BOUCHER, C.A.B., LEONARD, J.M., NORBECK, D.W. & KEMPF, D.J. 1996. Ordered accumulation of mutations in HIV protease confers resistance to ritonavir. *Nature medicine*, 2(7):760-766, Jul.

MOYNIHAN, C.T., EASTEAL, A.J., WILDER, J. & TUCKER, J. 1974. Dependence of the glass transition temperature on heating and cooling rate. *The journal of physical chemistry*, 78(26):2673-2677, Dec.

ROSSITER, D., *ed*. 2010. South African medicines formulary. 9th ed. Rondebosch, South Africa: health and medical publishing group. 639 p.

SAFRIN, S. 2004. Antiviral agents. (*In* Katzung, B.G., *ed*. Basic and clinical pharmacology 9th ed. Singapore: McGraw-Hill. p. 801-827)

SALEKI-GERHARDT, A., AHLNECK, C. & ZOGRAFI, G. 1994. Assessment of disorder in crystalline solids. *International journal of pharmaceutics*, 101(3):237-247, Jan.

SHAM, H.L., KEMPF, D.J., MOLLA, A., MARSH, K.C., KUMAR, G.N., CHEN, C.-M., KATI, W., STEWART, K., LAL, R., HSU, A., BETEBENNER, D., KORNEYEVA, M., VASAVANONDA, S., MCDONALD, E., SALDIVAR, A., WIDEBURG, N., CHEN, X., NIU, P., PARK, C., JAYANTI, V., GRABOWSKI, B., GRANNEMAN, G.R., SUN, E., JAPOUR, A.J., LEONARD, J.M., PLATTNER, J.J. & NORBECK, D.W. 1998. ABT-378, a highly potent inhibitor of human immunodeficiency virus protease. *Antimicrobial agents and chemotherapeutics*, 42(12):3218-3224, Dec.

VAN DEN MOOTER, G., WUYTS, M., BLATON, N., BUSSON, R., GROBET, P., AUGUSTIJNS, P. & KINGET, R. 2001. Physical stabilisation of amorphous ketoconazole in solid dispersions with polyvinylpyrrolidone K25. *European journal of pharmaceutical sciences*, 12(3):261-269, Jan.

VYAZOVKIN, S. & DRANCA, I. 2006. Probing beta relaxation in pharmaceutically relevant glasses by using DSC. *Pharmaceutical research*, 23(2):422-428, Feb.

WALMSLEY, S., BERNSTEIN, B., KING, M., ARRIBAS, J., BEALL, G., RUANE, P., JOHNSON, M., JOHNSON, D., LALONDE, R., JAPOUR, A., BRUN, S., SUN, E. & THE M98-863 STUDY TEAM. 2002. Lopinavir-ritonavir versus nelfinavir for the initial treatment of HIV infection. *The New England journal of medicine*, 346(26):2039-2046, Jun.